Earth-Science Reviews 200 (2020) 102964

Contents lists available at ScienceDirect

Earth-Science Reviews

journal homepage: www.elsevier.com/locate/earscirev

Advancing Santorini's tephrostratigraphy: New glass geochemical data and improved marine-terrestrial tephra correlations for the past ~360 kyrs

Sabine Wulf[a,b,*], Jörg Keller[c], Christopher Satow[d], Ralf Gertisser[e], Michael Kraml[c,1], Katharine M. Grant[f], Oona Appelt[g], Polina Vakhrameeva[b], Andreas Koutsodendris[b], Mark Hardiman[a], Hartmut Schulz[h], Jörg Pross[b]

[a] School of the Environment, Geography and Geosciences, University of Portsmouth, Portsmouth, United Kingdom
[b] Paleoenvironmental Dynamics Group, Institute of Earth Sciences, Heidelberg University, Heidelberg, Germany
[c] Department of Mineralogy-Geochemistry, Institute of Earth and Environmental Sciences, University of Freiburg, Freiburg, Germany
[d] Department of Social Sciences, Oxford Brookes University, Oxford, United Kingdom
[e] School of Geography, Geology and the Environment, Keele University, Keele, United Kingdom
[f] Research School of Earth Sciences, The Australian National University, Canberra, Australia
[g] Helmholtz Centre Potsdam, GFZ German Research Centre for Geosciences, Section 3.6 Chemistry and Physics of Earth Materials, Potsdam, Germany
[h] Department of Geosciences, University of Tübingen, Tübingen, Germany

ARTICLE INFO

Keywords:
Santorini
EPMA glass chemistry
Proximal tephra deposits
Marine tephrostratigraphy
Land-sea correlations
Eastern Mediterranean region

ABSTRACT

The island of Santorini in the Aegean Sea is one of the world's most violent active volcanoes. Santorini has produced numerous highly explosive eruptions over at least the past ~360 kyrs that are documented by the island's unique proximal tephra record. However, the lack of precise eruption ages and comprehensive glass geochemical datasets for proximal tephras has long hindered the development of a detailed distal tephrostratigraphy for Santorini eruptions. In light of these requirements, this study develops a distal tephrostratigraphy for Santorini covering the past ~360 kyrs, which represents a major step forward towards the establishment of a tephrostratigraphic framework for the Eastern Mediterranean region. We present new EPMA glass geochemical data of proximal tephra deposits from twelve Plinian and numerous Inter-Plinian Santorini eruptions and use this dataset to establish assignments of 28 distal marine tephras from three Aegean Sea cores (KL49, KL51 and LC21) to specific volcanic events. Based on interpolation of sapropel core chronologies we provide new eruption age estimates for correlated Santorini tephras, including dates for major Plinian eruptions, Upper Scoriae 1 (80.8 ± 2.9 ka), Vourvoulos (126.5 ± 2.9 ka), Middle Pumice (141.0 ± 2.6 ka), Cape Thera (156.9 ± 2.3 ka), Lower Pumice 2 (176.7 ± 0.6 ka), Lower Pumice 1 (185.7 ± 0.7 ka), and Cape Therma 3 (200.2 ± 0.9 ka), but also for 17 Inter-Plinian events. Older Plinian and Inter-Plinian activity between ~310 ka and 370 ka, documented in the distal terrestrial setting of Tenaghi Philippon (NE Greece), is independently dated by palynostratigraphy and complements the distal Santorini tephrostratigraphic record.

1. Introduction

Tephra (volcanic ash) layers in sedimentary records have long been used as dating tools in Quaternary science (e.g., Thorarinsson, 1944; Lowe, 2011) and are today widely applied for synchronising palaeoclimate proxy datasets on regional to supra-regional scales (e.g., Lane et al., 2013; Wulf et al., 2013; Rach et al., 2014). However, an important prerequisite for reliable dating and proxy-data linking via tephras is the availability of detailed tephrostratigraphic frameworks for volcanic eruption centres. Ideally, these tephrostratigraphies encompass complete sequences of past eruptive events in stratigraphic order, high-precision dating, and comprehensive glass geochemical datasets of erupted tephras from proximal (i.e., near-vent) settings that enable detailed correlations with distal deposits. In Europe, such tephrostratigraphies are well established for Holocene and Lateglacial Icelandic volcanoes (e.g., Larsen and Eiriksson, 2008; Lawson et al., 2012; Davies et al., 2014; Gudmundsdóttir et al., 2016; Wastegård et al., 2018) and for the Italian volcanic peninsula dating back to ~800 ka (e.g., Narcisi and Vezzoli, 1999; Wulf et al., 2004; Santacroce et al., 2008; Zanchetta et al., 2011; Wulf et al., 2012; Insinga et al., 2014; Albert et al., 2017; Giaccio et al., 2017a). In contrast,

* Corresponding author at: School of the Environment, Geography and Geosciences, University of Portsmouth, Portsmouth, United Kingdom.
E-mail address: sabine.wulf@port.ac.uk (S. Wulf).
[1] Present address: Geothermal Engineering GmbH, Surface Exploration and Research, Karlsruhe, Germany.

https://doi.org/10.1016/j.earscirev.2019.102964
Received 1 May 2019; Received in revised form 14 September 2019; Accepted 20 September 2019
Available online 24 October 2019
0012-8252/

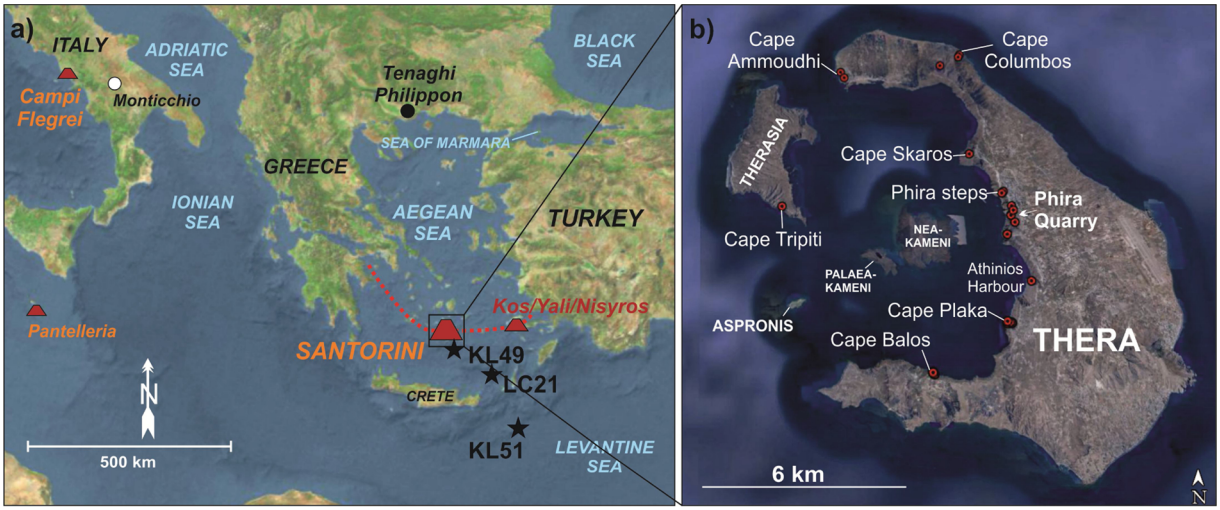

Fig. 1. (a) Topographic map of the Eastern Mediterranean region with locations of volcanoes and terrestrial sites of Lago Grande di Monticchio and Tenaghi Philippon (filled circles). Black stars indicate the positions of marine cores KL49, LC21 and KL51. Red dotted line shows the position of the southern Aegean volcanic arc. **(b)** Inlet satellite image of Santorini (Google Earth, 2018) with main proximal tephra sampling sites (see more details in Supplementary material S1) (For interpretation of the references to colour in this figure legend, the reader is referred to the web version of this article.).

tephrostratigraphies are still fragmentary for the Eastern Mediterranean region. This applies particularly to Aegean Arc volcanoes and notably Santorini Island, which hosts one of the world's most explosive, still active volcanic centres (e.g., Druitt et al., 1999). Santorini volcanism is particularly well known for its Late Bronze Age or Minoan eruption at ~1600 BC, which represents one of the world's largest volcanic eruptions in recorded history (e.g., Bond and Sparks, 1976; Sparks and Wilson, 1990; Druitt et al., 1999; Friedrich et al., 2006). This eruption may have severely impacted the Late Minoan civilisation in the Aegean region, with massive pumice fall and pyroclastic density currents (PDCs) destroying the town of Akrotiri on Thera (Santorini) and a tsunami devastating coastal towns on the nearby island of Crete (e.g., Marinatos, 1939; Antonopoulos, 1992; Friedrich, 2000; Bruins et al., 2008).

The proximal tephra record on Santorini documents numerous Plinian and Inter-Plinian eruptions during the past ~360 kyrs, but dating of the calc-alkaline products (tephras) from these eruptions has long been challenging, especially beyond the radiocarbon dating range. This is because most radioisotopic dates derived from whole-rock K/Ar and multi-grain $^{40}Ar/^{39}Ar$ methods produced large age uncertainties due to either inherited feldspar xenocrysts and the generally low K-contents of Santorini eruption products (~0.1–3.8 wt% K_2O; Druitt et al., 1999), or high atmospheric contamination (on average > 95%; Fabbro et al., 2013). Furthermore, the low number of macroscopically visible Santorini tephras in distal settings such as in deep-sea cores from the Aegean and Levantine Seas (Keller et al., 1978; Federman and Carey, 1980; Vinci, 1985) did not stimulate tephrostratigraphic studies in this region for a long time, leading to a focus of Santorini tephra on petrographical and bulk rock geochemical characterisation rather than on glass compositions (e.g., Fouqué, 1879; Reck, 1936; Druitt et al., 1999; Vespa et al., 2006; Gertisser et al., 2009). Hence, EPMA glass geochemical data available from the proximal record are either published as mean data (Federman and Carey, 1980; Keller, 1981; Vinci, 1985; Druitt et al., 1999; Gertisser et al., 2009) or comprise only major eruptive units of the last ~100 kyrs (Tomlinson et al., 2015), highlighting a need for a new comprehensive dataset.

Recent tephrostratigraphic studies of marine core LC21 from the SE Aegean Sea (Satow et al., 2015) identified for the first time macroscopically non-visible (crypto)tephra layers of Santorini provenance in the Eastern Mediterranean Sea. However, due to the lack of comparative glass geochemical data, these cryptotephras have not yet been correlated to specific volcanic events (Satow et al., 2015), which currently limits their use as isochronous marker layers.

In recognition of the need of a comprehensive glass geochemical dataset, systematic sampling and EPMA major-element analysis of all Plinian and a number of Inter-Plinian deposits from the proximal tephra record on Santorini has been carried out for this study. The new dataset has been employed to assign precise eruptions to the above-mentioned (crypto)tephra dataset from core LC21 (Satow et al., 2015) and to the visible tephra records of two other important Aegean Sea cores, namely cores M40/4-65 (GeoTÜ-KL49; hereafter: KL49) and M40/4-67 (GeoTÜ-KL51; hereafter: KL51), to provide a complete marine-distal Santorini tephrostratigraphic framework for the region southeast of Santorini for the last 200 kyrs (Schwarz et al., 1999; Keller et al., 2000; Schwarz, 2000). Furthermore, the original age models of cores KL49 and KL51 as used by Schwarz (2000) and Keller et al. (2000) for estimating ages for marine Santorini tephras have been revised using the latest chronological information available for sapropel boundaries and other tephra markers. Independent dates for older Santorini Plinian and Inter-Plinian activity between ~310 and 370 ka have been derived through palynostratigraphic age constraints of several cryptotephra layers in the distal terrestrial archive of Tenaghi Philippon, NE Greece (Vakhrameeva et al., 2018, 2019).

The new, ~360-kyr-long distal tephrostratigraphic record for Santorini facilitates reliable correlations of future Santorini-derived (crypto)tephra findings in marine and terrestrial palaeoenvironmental archives from the Eastern Mediterranean region. It furthermore helps to recognise Santorini events that are not preserved in the proximal record and provides new insights into Santorini's past eruptive behaviour, including the frequency and dynamics of large explosive events as well as tephra dispersal patterns, which are crucial for understanding and estimating the nature and frequency of future eruptive events.

2. Santorini's eruptive history: the proximal record

Santorini is the largest and most active Quaternary volcanic centre within the southern Aegean volcanic arc (Fig. 1), which formed as a consequence of N-dipping subduction of the African plate underneath the European plate since the Miocene (e.g., Angelier et al., 1982; Mercier et al., 1989). Santorini consists of three major islands, Thera, Therasia and Aspronisi, which encircle the central flooded caldera with the youngest twin islands of Palaea and Nea Kameni (Fig.1). The Santorini volcanic complex, which formed over the last ≥650 kyrs (Druitt et al., 1999), overlies a ca. 20–30 km thick continental crust of Mesozoic and Cenozoic metamorphic rocks (e.g., Tartaris, 1964; Makris,

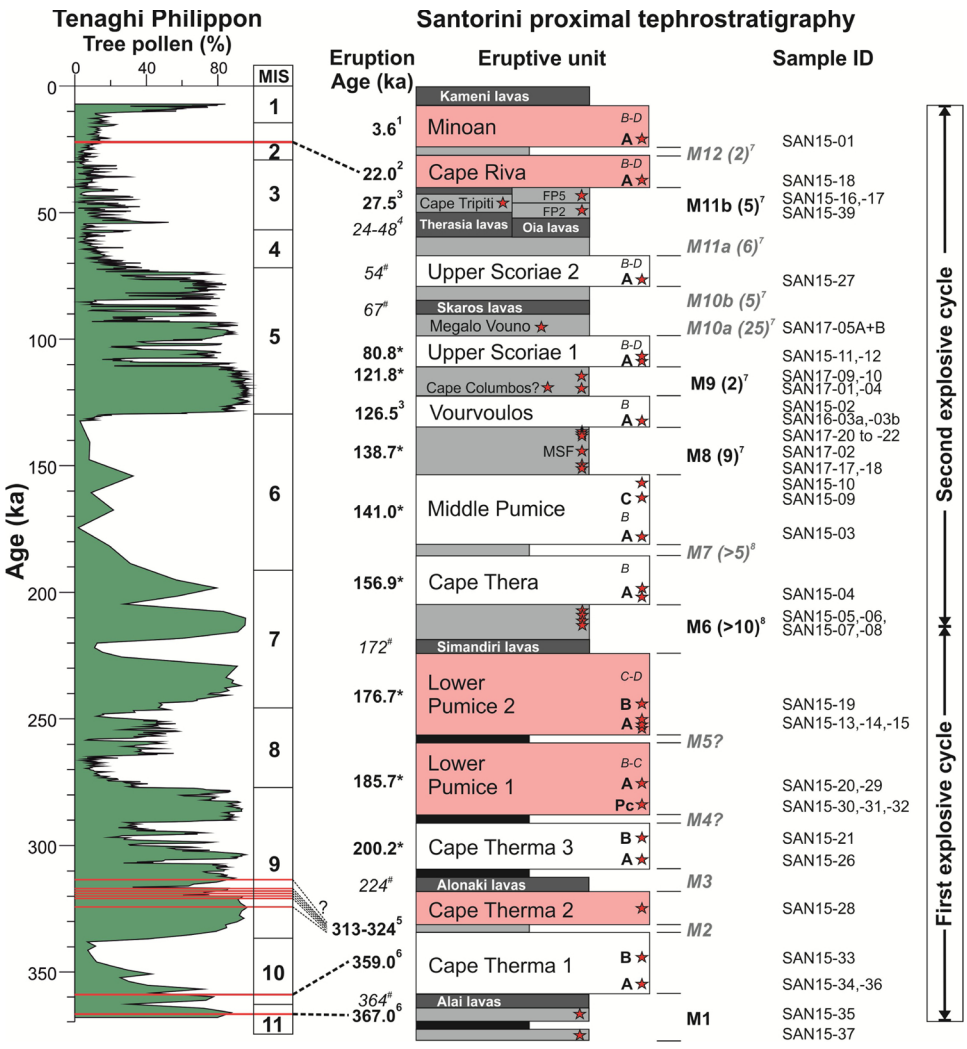

Fig. 2. Left: Tree-pollen curve of the Tenaghi Philippon peat record (NE Greece) for the past ca. 370 kyrs with positions of Marine Isotope Stages (MIS) and (crypto)tephra layers of Santorini provenance (red lines). Data from Pross et al. (2009, 2015), Müller et al. (2011); Fletcher et al. (2013); Milner et al. (2016); Wulf et al. (2018), and Vakhrameeva et al. (2018, 2019). Right: Revised Santorini proximal eruptive history showing Plinian events (white fields = intermediate composition, red field = silicic composition), Inter-Plinian activity (light grey fields), lava-shield (dark grey fields) and soil formation (black fields); modified after Druitt et al. (1999). Ages of eruptions are obtained from: [1] Friedrich et al. (2006), [2] Bronk Ramsey et al. (2015), [3] Satow et al. (2015), [4] Fabbro et al. (2013), [5] Vakhrameeva et al. (2019), [6] Vakhrameeva et al. (2018), [#] Druitt et al. (1999) and * this study. Red stars show the stratigraphic position of proximal tephra samples taken for this study, and respective tephra sample IDs are listed on the right. Inter-Plinian (M) deposits in bold indicate intervals that have been analysed in this study. Numbers in brackets behind M deposits indicate the number of recognised Inter-Plinian units as estimated by [7] Vespa et al. (2006) and [8] Edwards (1994). Note that this number is not representative for the number of distinct eruptions (For interpretation of the references to colour in this figure legend, the reader is referred to the web version of this article.).

1978; Li et al., 2003; Druitt et al., 2015). Early shallow-marine to subaerial volcanic activity produced dacitic to rhyodacitic lava flows from centres of the Akrotiri Peninsula in the southwest of Thera Island (Druitt et al., 1999). These were followed by effusive and minor explosive activity from the basaltic-andesitic Peristeria composite volcano in northern Thera (530 – 430 ka; Druitt et al., 1999). Commencing around the time of the last Peristeria activity, cinder and spatter cones were formed by Strombolian eruptions on the Akrotiri Peninsula (450 – 340 ka; Druitt et al., 1999).

Major explosive volcanism started at ~360 ka; to date, this has resulted in twelve major Plinian (Druitt et al., 1989, 1999) and numerous Inter-Plinian explosive eruptions (labelled M1 to M12) that have yet been rarely and only selectively studied (e.g., Edwards, 1994; Druitt et al., 1999; Vespa et al., 2006; Fabbro et al., 2013) (Fig. 2). Pumice and scoria deposits from these events form the Thera Pyroclastic Formation (TPF) that is well exposed in the caldera wall succession of the Santorini ring islands. The TPF has been subdivided into two explosive cycles based on long-term trends in magma composition, with each cycle starting with mafic to intermediate magmas and ending with a silicic, caldera-forming eruption (Druitt et al., 1999). During the first explosive cycle between ~360 and 180 ka, five Plinian eruptions took place, preceded and intercalated by minor explosive eruptions and lava-shield formations at Cape Alai (364 ± 62 ka; Druitt et al., 1999) and Cape Alonaki (224 ± 5 ka; Druitt et al., 1999) (Fig. 2). The oldest Plinian eruptions produced the andesitic and rhyodacitic pyroclastic successions of Cape Therma 1 (CTM1), Cape Therma 2 (CTM2), and Cape Therma 3 (CTM3). The eruption ages of CTM1 and CTM2 are roughly constrained to ≤360 ka and ~225 ka based on $^{40}Ar/^{39}Ar$ dates of directly underlying Cape Alai (CTM1) and overlying Cape Alonaki lavas (CTM2), respectively (Druitt et al., 1999) (Fig. 2). A first age estimate for the CTM3 eruption of 196 ka was derived from interpolation of the proposed marine tephra correlative "Intra-S7″ by the original age model of Aegean Sea core KL51 (Keller et al., 2000; Schwarz, 2000). The Cape Therma successions are overlain by the rhyodacitic Lower Pumice 1 (LP1) and Lower Pumice 2 (LP2) deposits (e.g., Druitt et al., 1989, 1999; Gertisser et al., 2009; Simmons et al., 2016), both formerly assigned to the "Unterer Bimsstein" (Reck, 1936) or "Lower Thera Pumice" (Keller, 1981). LP1 and LP2 were derived from relatively closely spaced Plinian events that are separated by a thin palaeosol. LP1 and LP2 have been proposed to be distally recorded in the KL51 marine record as V-3 and V-1 tephras, where their ages were interpolated at 184 and 172 ka, respectively (Keller et al., 1978, 2000, 2014; Schwarz, 2000). The LP2 eruption resulted in the collapse of Caldera 1 (Druitt et al., 1989, 1999; Gertisser et al., 2009), and was followed by the formation of the Simandiri lava-shield (172 ± 4 ka; Druitt et al., 1999). Minor deposits of Inter-Plinian activity (M1 to M5) have been noted for the first explosive cycle, but have yet remained scarcely investigated (Edwards, 1994; Druitt et al., 1999).

The second explosive cycle (~180 – 3.6 ka) started with the eruption of the Middle Tuff Series, which encompasses andesitic to dacitic fall deposits and PDC deposits (ignimbrites) from four major Plinian eruptions. These include the Cape Thera (CTA), Middle Pumice (MP), Vourvoulos (V) and Upper Scoriae 1 (USC1) eruptions, all of which are intercalated by relatively thick, mafic to intermediate ash and scoria

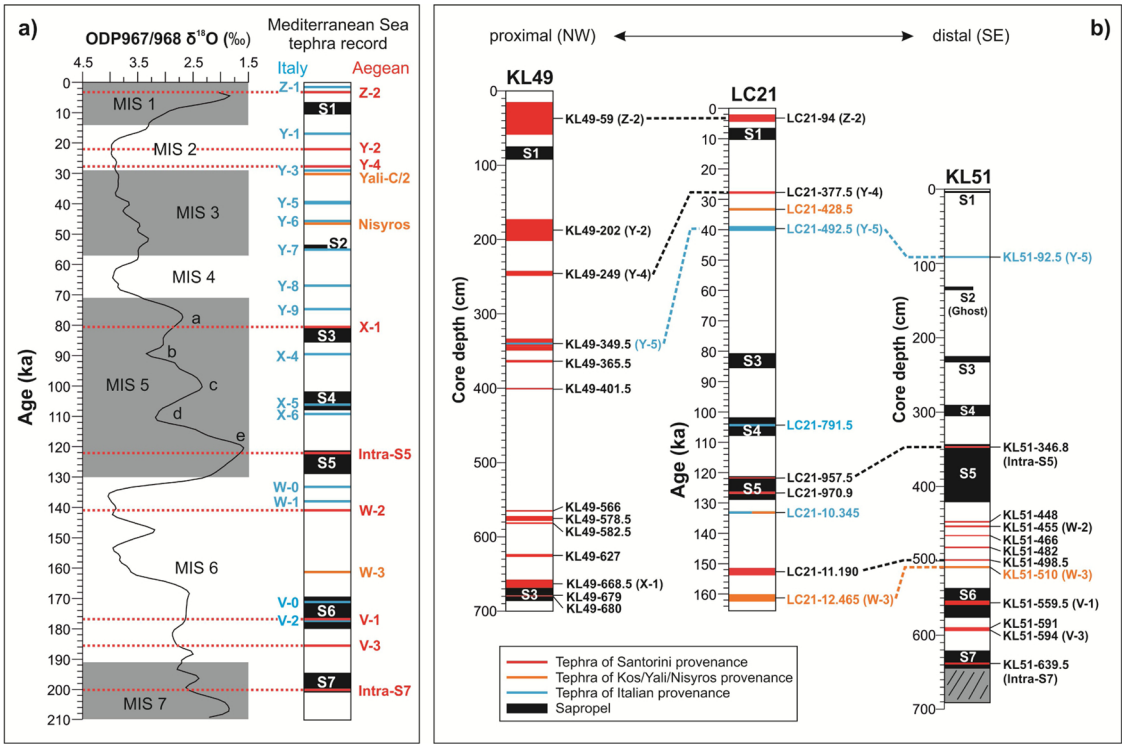

Fig. 3. (a) Benthic oxygen-isotope splice from ODP Sites 967/968 in the Eastern Mediterranean Sea (Konijnendijk et al., 2015) with positions of marine isotope stages (left) and revised Eastern Mediterranean marine tephrostratigraphic record for the last ~210 kyrs (right). Time constraints for sapropels S1 to S7 are from Grant et al. (2016, 2017). **(b)** Sediment logs of marine cores KL49, LC21 and KL51 with positions of tephra layers analysed and discussed in this study adapted from Hieke et al. (1999), Schwarz (2000), and Satow et al. (2015) (For interpretation of the references to colour in this figure legend, the reader is referred to the web version of this article.).

beds from Inter-Plinian events (M6 to M10; Druitt et al., 1999; Vespa et al., 2006). The Skaros caldera (Caldera 2) formed incrementally during the eruptions of the Middle Tuff Series and was established after the USC1 event. It was subsequently filled by the lava flows of the Skaros lava shield (67 ± 9 ka; Druitt et al., 1999) in the northern part of Thera. Deposits of Plinian and Inter-Plinian eruptions of the Middle Tuff Series all lack radioisotopic dating, but the first interpolated age estimates from marine sapropels indicate eruption ages of 144.6 ± 2 ka for MP (marine W-2 tephra) and 80 ± 2 ka for USC1 (marine X-1 tephra; Keller et al., 2000; Schwarz, 2000).

The time interval of the eruption of the Middle Tuff Series has also been considered for the formation of the Megalo Vouno cinder cone and Cape Columbos tuff ring that occurred along the NE-SW striking Columbos tectonic line in NE Thera (Druitt et al., 1999). Reliable radioisotopic ages for these eruptions are not yet available; however, the stratigraphic position of the Megalo Vouno scoria deposits relative to Plinian deposits of the Middle Tuff Series suggests a timing of this event between the Vourvoulos eruption and the Skaros lava-shield formation (Druitt et al., 1999; Vespa et al., 2006). Furthermore, petrological similarities suggest an even more specific allocation within the early M10a Inter-Plinian interval, i.e., after the eruption of USC1 and prior to the Skaros lavas (Vespa et al., 2006). The phreatomagmatic nature of the Cape Columbos tuff ring, on the other hand, implies that this likely formed at a time when sea level was comparable to today's, i.e. during the last interglacial period (MIS 5e; Druitt et al., 1999).

The Middle Tuff Series and the Skaros lava shield are succeeded by the andesitic deposits of the major Upper Scoriae 2 eruption (USC2) that is dated by several means, i.e. by K/Ar whole rock at 79 ± 8 ka, by $^{40}Ar/^{39}Ar$ whole rock at 54 ± 3 ka (Druitt et al., 1999), and by radiocarbon determinations on organic material underlying the USC2 deposit at 37.9 ± 0.2 ^{14}C ka BP (Mellors and Sparks, 1991). The USC2 event is followed by the extrusion of rhyodacitic lavas forming the Therasia dome complex exposed on Therasia and Thera (48 – 24 ka; Fabbro et al., 2013), and the thin andesitic lava flows at Oia in northern Thera that occur in the same stratigraphic level as the Therasia lavas. On Therasia, the upper part of the lava succession is intercalated by the silicic Cape Tripiti pumice deposit (26 ka; Fabbro et al., 2013). At Cape Ammoudhi in northern Thera, five discrete, thin pumice fall deposits (FP1 to FP5) overly the Oia lavas (Vespa et al., 2006); their chronostratigraphic relationship to the Cape Tripiti Pumice is yet unclear.

The second explosive cycle terminated with the two rhyodacitic, caldera-forming Cape Riva (CR, Caldera 3; Druitt and Sparks, 1982; Druitt, 1985) and the Late Bronze Age or Minoan eruptions (MIN, Caldera 4; e.g., Bond and Sparks, 1976; Sparks and Wilson, 1990; Druitt et al., 1999) (Fig. 2). Both eruptions formed prominent pyroclastic fall and PDC deposits, and are radiocarbon-dated at 22.0 ± 0.6 cal ka BP (2σ uncertainty; Pichler and Friedrich, 1976; Bronk Ramsey et al., 2015) and 1613 ± 13 cal a BC (3563 ± 13 cal a BP; Friedrich et al., 2006), respectively. Historic effusive activity has built the present-day islands of Palaea Kameni and Nea Kameni, with the last eruption taking place in AD 1950 (Fytikas et al., 1990).

3. Santorini's distal tephrostratigraphic record: state of the art

Explosive activity on Santorini during at least the last ~360 kyrs has produced large volumes of fallout tephra in the proximal record, and hence has the potential for distal dispersal. Research on Santorini's distal tephrostratigraphy was initiated in the 1960s by the first detection of the Minoan (Z-2) tephra in Eastern Mediterranean deep-sea sediments (e.g., Ninkovich and Heezen, 1965, 1967; Keller and Ninkovich, 1972; Keller et al., 1978; Watkins et al., 1978; Vinci, 1985), on the islands of Crete, Milos and Rhodes (e.g., Vitaliano and Vitaliano, 1974; Doumas and Papazoglou, 1980; Bruins et al., 2019), and in Asia Minor (e.g., Sullivan, 1988). Subsequent studies of marine sediment cores from the southern Aegean and Levantine Seas identified six further visible tephra layers of Santorini provenance in deeper

stratigraphic positions that, according to their occurrence in different foraminiferal stratigraphic zones, are labelled as Y-2 (CR), Y-4 (Cape Tripiti), X-1 (USC1), W-2 (MP), V-1 (LP2) and V-3 (LP1) tephras (e.g., Keller et al., 1978; Federman and Carey, 1980; Vinci, 1985; Fabbro et al., 2013) (Fig. 3).

During the past two decades, new findings at distal marine, but also at terrestrial sites from the northern Aegean Sea region (e.g., St. Seymour et al., 2004; Margari et al., 2007; Aksu et al., 2008; Wulf et al., 2018), the Sea of Marmara (e.g., Wulf et al., 2002; Çağatay et al., 2015), the Black Sea (Guichard et al., 1993; Kwiecien et al., 2008; Cullen et al., 2014), and Turkey (e.g., Eastwood et al., 1999; Roeser et al., 2012; Sulpizio et al., 2013) have extended the known dispersal fan of the younger Z-2 and Y-2 tephras. However, this does not hold true for older distal marker tephras (i.e., X-1, W-2, V-1, V-3). Notably, all distal findings have so far been restricted to macroscopically visible layers of the above-mentioned eruptions, hence providing no new insights into the eruption dynamics and tephra dispersal patterns of other, likely less energetic Santorini eruptive events.

Satow et al. (2015) demonstrated for the first time the potential of detailing the distal Santorini tephrostratigraphic record through the systematic cryptotephra analysis of core LC21 from the SE Aegean Sea spanning the past ~160 kyrs (Fig. 3). Furthermore, ongoing studies of the long Tenaghi Philippon (TP) peat sequence in NE Greece have highlighted the presence of older Santorini cryptotephras, some of which have been correlated with the Cape Therma 1 eruption, and M1 and M2 Inter-Plinian activity based on the proximal Santorini glass dataset presented here (Vakhrameeva et al., 2018, 2019) (Fig. 2).

The first Santorini cryptotephra findings in palaeoclimate archives of the Aegean region mark a turning point in the development of a more detailed Santorini tephrostratigraphy, but also highlight the need for a comprehensive proximal Santorini glass geochemical dataset for reliable tephra correlations.

4. Material and methodologies

4.1. Sampling and analysis of proximal tephras from Santorini

For this study, the sampling of proximal Santorini tephra deposits concentrated on pyroclastic fall units in order to facilitate correlations with air-borne distal tephra layers.

In total, 49 tephra samples were taken during three field campaigns on Santorini in September 2015, November 2016 and April 2017 (samples "SAN15", "SAN16" and "SAN17", respectively). Sampling encompassed mainly the basal fall units of all twelve major Plinian and 25 of the most prominent fall units of the M11b, M9, M8, M6 and M1 Inter-Plinian intervals, including deposits from the Megalo Vouno cinder cone and the Cape Columbos tuff ring. In addition to basal fall units, samples from PDC (ignimbritic) sub-units of three of the older Plinian eruptions (CTM1, CTM3, and LP2) have been taken since those could have potentially produced distal co-ignimbritic ash fall with different glass chemical compositions. This may also hold true for PDC units of other Plinian eruptions, i.e., LP1, CTA, MP, V, USC1, and USC2, which have not been sampled for this study. However, in order to guarantee reliable marine tephra correlations with their proximal counterpart, unpublished USC2-B glass data of Schwarz (2000) and mean EDS analyses of other relevant missing PDC units from Druitt et al. (1999) have been taken into account for comparison (Figs. 7–9).

For this study, most of the sampled proximal tephra fall deposits were accessible at the caldera cliffs of Thera (e.g., Cape Ammoudhi, Cape Plaka, Cape Balos, Phira Steps) and Therasia (Cape Tripiti), or at road cuts and quarries (e.g., Phira Quarry). Details of all sampling sites are provided in Supplementary material S1.

Representative juvenile clasts (pumice and scoria fragments) were sampled vertically across the individual deposits, then rinsed in the laboratory with deionized water, dried, crushed and sieved. Glassy material from the 20–100 μm (SAN15 samples) and 25–125 μm (SAN16 and SAN17 samples) fractions was embedded in resin (Epofix), sectioned and polished for geochemical analysis.

The major element composition of individual glass shards from samples SAN15 (n > 20) was obtained by electron probe microanalyses (EPMA) at the GFZ German Research Centre for Geosciences in Potsdam using a JEOL-JXA 8320 (WDS) probe with five spectrometers. Analytical setups during these measurements were 15 kV accelerating voltage and a 10 nA beam current, and a 5–10 μm beam was used (Supplementary material S2). Count times per element were 20 s for Fe, Mn, Ti, Mg, P, and Cl, and 10 s for Si, Al, K, Ca, F, and Na (measured first). Instrumental calibration and data quality verification prior to sample analyses used common mineral standards, Max Planck Institute (MPI) glass standards ATHO-G, StHs6/80 and GOR-132 (Jochum et al., 2006), and the natural Lipari obsidian (Hunt and Hill, 1996; Kuehn et al., 2011).

Major element glass concentrations of SAN16 and SAN17 samples were measured at the Natural History Museum, London. Analytical conditions used a 5-spectrometer CAMECA SX100 microprobe with an accelerating voltage of 20 kV, a beam current of 20 nA and a defocused beam of 10 μm diameter in order to minimise volatile loss. Count times per element were 30 s except for Na (12 s, and measured first), P and Mn (60 s), and Cl (50 s). MPI glass standards StHs6/80 and ATHO-G (Jochum et al., 2006) were analysed at the start, during and at the end of each run to monitor analysis accuracy and precision. Analytical data of SAN15, SAN16 and SAN17 samples were filtered to remove analyses of non-vitreous material (i.e., microlites) and those that yielded analytical totals lower than 95 wt% (mafic-intermediate compositions) and 90 wt% (rhyolitic glass compositions), respectively. For data comparison in bivariate elemental plots (Figs. 5, S1-3, S1-8, S1-11, S1-14, S1-19 and S1-22 in Supplement material S1) analytical data were normalised to 100 wt%. All raw and normalised geochemical data including glass standard data are provided in Supplementary material S2.

4.2. Sampling and analysis of distal marine tephras

4.2.1. Deep-sea cores KL49 and KL51 (SE Aegean Sea)

During R/V METEOR cruise M40/4 in January 1998, several deep-sea cores were collected from the Aegean Sea for palaeoceanographic investigation (Hieke et al., 1999). Two of these cores, KL49 and KL51 (M40/4-65 and M40/4-67 in Hieke et al., 1999), from medial-distal to distal locations southeast of Santorini (Fig. 1) were tephrochronologically analysed by Schwarz (2000), and respective data are presented here. Cores KL49 and KL51 have been chosen for this study because they contain (1) numerous macroscopically visible tephra layers, (2) well-preserved sapropels, and (3) undisturbed sediments with very limited indications of reworking (e.g., turbidites) and bioturbation. All these criteria are important for constructing reliable age models and eventually developing precise tephrostratigraphies.

Piston core KL49 was retrieved from a morphological high at 827 m water depth, ca. 30 km south-southeast of Santorini (N36°08′46.2″, E25°33′51.6″). Core KL51 was recovered from a trough in 2158 m water depth, ca. 250 km southeast of Santorini (N34°48′49.8″, E27°17′46.2″). The cores comprise 7 m and 6.91 m of marine sediments and extend back to sapropels S3 (KL49; ~87 ka) and S7 (KL51; ~200 ka), respectively (see Hieke et al., 1999, for detailed core descriptions).

Glass geochemical data of 13 (KL49) and ten (KL51) Santorini tephras, in addition to two other-sourced tephras from Schwarz (2000), have been used for this study and labelled according to their core name and basal depth in cm, for example KL49-59 (Fig. 3; Supplementary material S3). Marine tephra samples were sieved into 36–150 μm grain size fractions, and liquid density and magnetic separation were applied to remove magnetic minerals and organic material. Geochemical compositions of tephra glass shards were determined by a CAMECA SX100 electron microprobe (WDS) at Institute of Earth and Environmental Sciences, Freiburg (Germany), using a 15 kV accelerating voltage, 10 nA beam current, and a defocused beam of 10 μm diameter

(Supplementary material S3). Peak counting times for each element were 20 s except for Na, which was analysed first at 10 s. Instrumental calibration used International mineral and obsidian standards such as USNM 7285, KN18, and KE12 (Nielsen and Sigurdsson, 1981; Devine et al., 1995). Comparable methods as for the proximal glass dataset were applied for filtering and normalising major element data of marine tephras (Figs. 7–9, Supplementary material S3).

4.2.2. Deep-sea core LC21 (SE Aegean Sea)

Core LC21 was collected in 1995 during Marion Dufresne cruise 81 from 1522 m water depth, ca. 130 km southeast of Santorini (N35°40′, E26°35′) (e.g., De Rijk et al., 1999; Hayes et al., 1999). Sedimentological and geochemical studies of this ~14 m long core have shown that it is excellently suited for high-resolution palaeoceanographic reconstructions for the past ~160 kyrs (e.g., Rohling et al., 2002, 2004; Casford et al., 2003; Marino et al., 2007, 2009; Abu-Zied et al., 2008; Grant et al., 2012, 2016). Furthermore, LC21 documents several visible tephra layers from Italian and Aegean Arc eruptions, and it is the first marine record in the Eastern Mediterranean Sea that has been studied for its cryptotephra content (Satow et al., 2015). A total of three visible and two cryptotephra layers has been geochemically assigned to Santorini eruptions (Fig. 3), three of which still lack detailed correlations (Satow et al., 2015). Labelling used the same approach as for tephras in the KL49 and KL51 cores (Figs. 7–9, Supplementary material S3).

4.3. Comparability of proximal and marine distal EPMA glass data

The new Santorini proximal tephra glass dataset was used for detailed correlations with the glass chemical data of marine tephras from cores KL49, KL51 (Schwarz, 2000; this study) and LC21 (Satow et al., 2015). However, proximal and marine tephras have been analysed by using four different instruments with different analytical setups (Table 1), and hence the level of comparability of data needs to be tested. The common use of glass standards for ensuring EPMA data quality and comparability (e.g., Kuehn et al., 2011; Lowe et al., 2017), is in this study, however, complicated by the fact that different glass standards were used during older (Freiburg) and recent measurements (GFZ Potsdam, NHM London, Oxford) (Table 1). Therefore, EPMA data of the proximal Vourvoulos fall (V-A) tephra have been used to evaluate elemental difference within a mutual sample measured by all four laboratories (Fig. 4). The comparison shows, on the one hand, that the new proximal glass datasets from the GFZ Potsdam and NHM London laboratories agree well with each other except for slight deviation in SiO_2, Na_2O and P_2O_5 values (Fig. 4). The Oxford data by Tomlinson et al. (2015) that used the same analytical setup as for the marine LC21 tephras (Satow et al., 2015) deviate from the more homogeneous GFZ Potsdam data but overlap with the more scattered data of NHM London data (Fig. 4). On the other hand, an unpublished glass dataset of the Vourvoulos proximal tephra from Schwarz (2000) that used the same EPMA instrumental setups as for marine KL49 and KL51 tephras (Freiburg) shows significant deviations in Na_2O and P_2O_5 values and slightly higher SiO_2 concentrations compared to the new EPMA datasets (GFZ Potsdam, NHM London) but agrees well for other elements, including TiO_2, FeO, MgO, CaO and K_2O (Fig. 4). The deviations in SiO_2 and Na_2O are interpreted as a result from Na-loss during EPMA measurements at the Freiburg instrument, and hence these elements have been either excluded (Na_2O) or handled with caution (SiO_2) for proximal-distal tephra correlations. In order to accommodate the comparability of SiO_2 data (one of the most important element for tephra identification), we have included the unpublished proximal dataset of (Schwarz, 2000) in all bivariate elemental plots next to the GFZ Potsdam and/or NHM London proximal data. This allowed for the more precise assignment of KL49 and KL51 marine tephras to their proximal counterparts (Figs. 7–9).

4.4. Chronological constraints of marine Santorini tephras

Correlations of glass geochemical data of proximal Santorini deposits with distal-marine tephra layers have not only allowed for detailed assignments to specific Santorini eruptive events but have also provided new or improved dating of tephras by marine sediment chronologies (Table 2). However, the accuracy and precision of tephra/eruption ages derived this way strongly depends on the reliability and resolution of the sediment core chronologies. The LC21 age model, for example, is based on aligning its high-resolution planktonic foraminiferal oxygen isotope data with the U/Th-dated Soreq cave speleothem $\delta^{18}O$ record (Bar-Matthews et al., 2000, 2003) and tie-pointing this correlation with radioisotopic ages of two tephra markers, Santorini's Minoan tephra and the Campanian Ignimbrite (Grant et al., 2012). This age model does not only enable precise dating of Santorini tephras (Satow et al., 2015), but also provides improved age estimates of sapropel S1 to S5 boundaries in the Eastern Mediterranean Sea (Grant et al., 2016). These and newly constrained ages of sapropels S6 and S7 from ODP Site 967 (Grant et al., 2017) as well as imported ages of firmly correlated tephra layers, including Z-2/Minoan, Y-2/Cape Riva, Y-4/Cape Tripiti, Y-5/Campanian Ignimbrite and W-3/Kos Plateau Tuff have been used to remodel the previously published chronological frameworks of cores KL49 and KL51 (Keller et al., 2000; Schwarz, 2000) (Fig. 5, Supplementary material S4). Linear interpolation of KL49 and KL51 chronologies was then applied to constrain eruption age estimates of marine Santorini tephras with 2σ analytical uncertainties (Table 2).

5. Glass compositions of proximal tephra deposits

Glass compositions (normalised to 100%) of proximal Santorini tephra fall (and minor flow) deposits demonstrate a wide range of either basaltic andesitic, andesitic, dacitic or rhyolitic chemistries which in most cases allow a distinction between individual Plinian and Inter-Plinian eruptive units (please see detailed descriptions in Supplement material S1). For example, glass compositions of the major silicic eruptions of Cape Therma 2, Lower Pumice 1 and 2, Cape Riva and Minoan as well as Inter-Plinian deposits M1 are distinguishable from each other on the basis of slight variations of their SiO_2, FeO, CaO and

Table 1
Summary of analytical setups (voltage, beam current, and beam size) for glass compositional data of Santorini tephras used for proximal-distal marine correlations in this study.

Laboratory	Instrument	Analytical setup	Glass standards	Samples analysed	Reference
GFZ Potsdam (WDS)	JEOL-JXA8320	15 kV, 10 nA, 5-10 µm	ATHO-G, StHs6/80, GOR-132, Lipari obs.	SAN15 (proximal)	This study
NHM London (WDS)	CAMECA- SX100	20 kV, 20 nA, 10 µm	ATHO-G, StHs6/80	SAN16, SAN17 (proximal: M9, V, M8, MV, CCT)	This study
Oxford University (WDS)	JEOL-JXA8600	15 kV, 6 nA, 10 µm	ATHO-G, StHs6/80	- LC21 (marine tephra) - V (proximal)	Satow et al. (2015) Tomlinson et al. (2015)
Freiburg University (WDS)	CAMECA-SX100	15 kV, 10 nA, 10 µm	KN18	KL49, KL51 (marine tephra), unpublished proximal tephra data	Schwarz (2000)

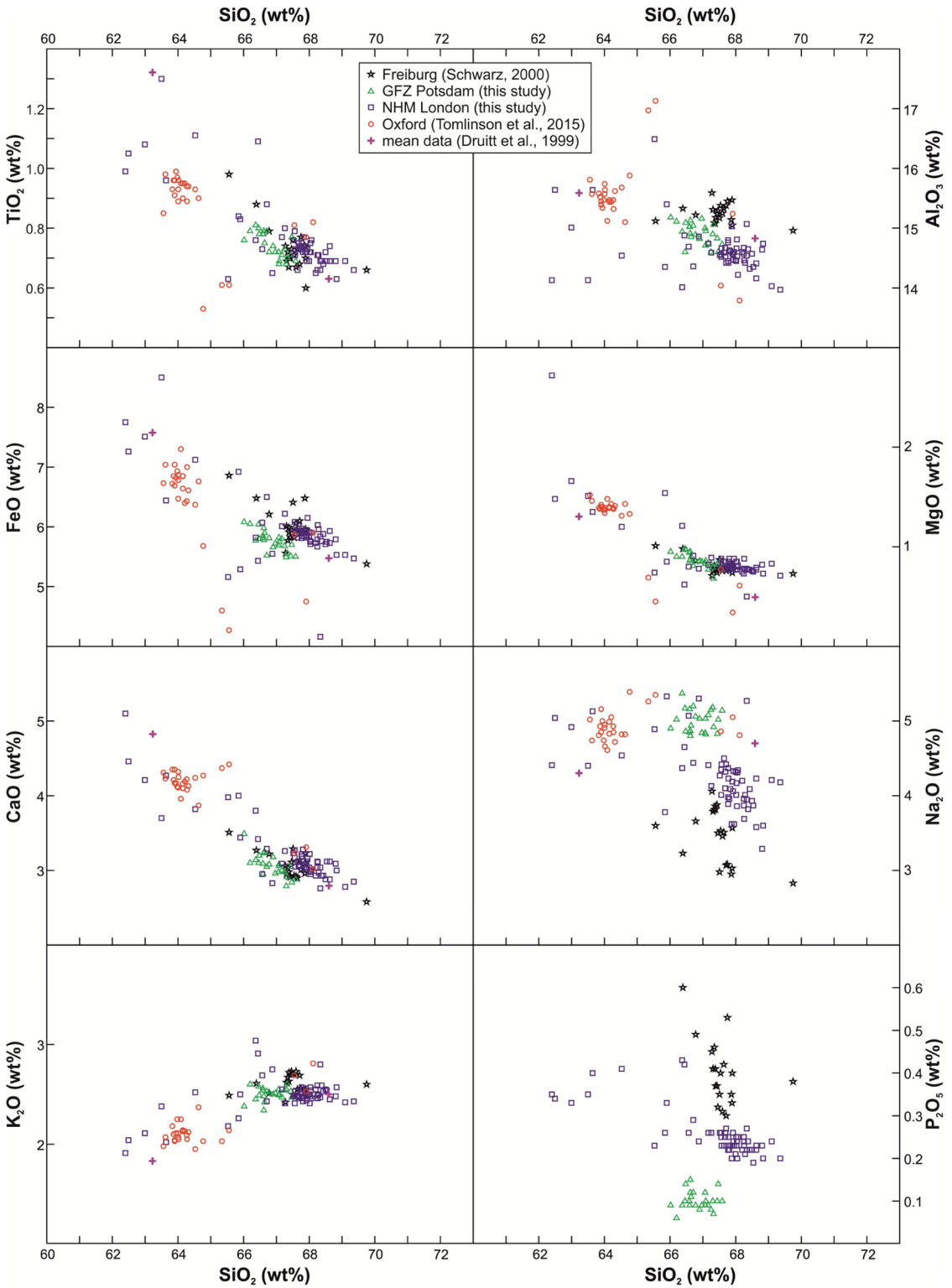

Fig. 4. Bivariate elemental plots of glass composition of the proximal Vourvoulos A fall deposits obtained by different microprobe instruments and analytical setups. Mean EDS glass data from Druitt et al. (1999) is also included for comparison.

alkali contents (Figs. 6, S1-3, S1-8, S1-22 in Supplement material S1). Tephras of intermediate (andesitic to dacitic) glass compositions, on the other hand, widely overlap within their major element chemistry and often do not allow a distinction just on the basis of their major element chemistry alone. This is especially the case for Plinian and some Inter-Plinian fall deposits of the Middle Tuff Series, i.e. Cape Thera, Middle Pumice, Vourvoulos, MSF and Upper Scoriae 1 (Figs. 6, S1-11, S1-14, S1-19). Rhyodacitic tephras of the M11b Inter-Plinian interval also have very similar major element glass compositions (Figs. 6, S1-22), indicating a potential correlation between the different sites in southern Therasia (Cape Tripiti Pumice) and at Oia in northern Thera, which, however, cannot be specified at this time.

Rather peculiar glass compositions have been found in the Cape Columbos (CCT) and Megalo Vouno (MV) deposits. Scoriae of the Cape Columbos Tuff have a dominantly basaltic andesitic glass chemistry and shows an additional very minor rhyolitic component at the top of the

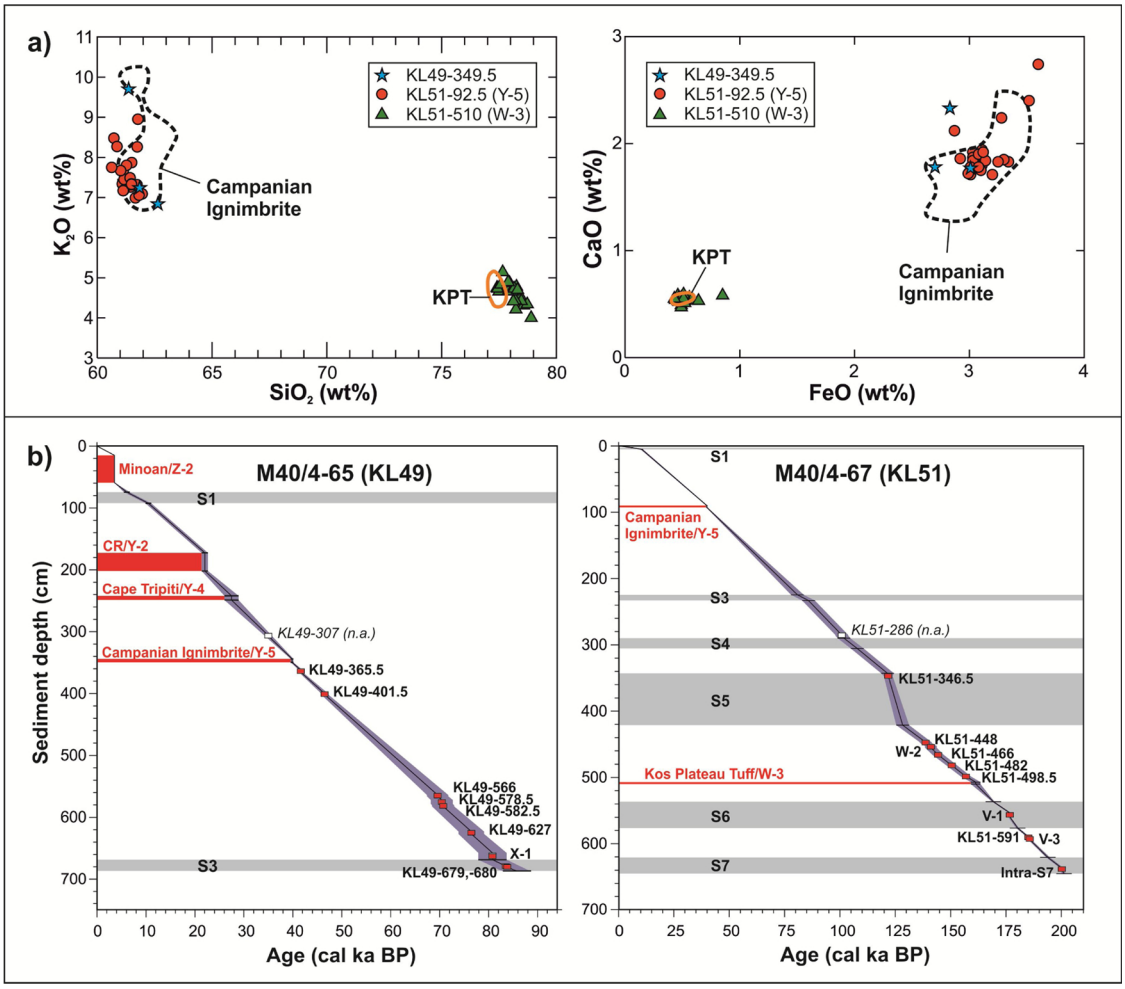

Fig. 5. (a) Bivariate plots of EPMA glass data of the marine Y-5/Campanian Ignimbrite and W-3/Kos Plateau Tuff (KPT) tephras occurring in cores KL49 and KL51 (this study; Schwarz, 2000). **(b)** Age-depth model of marine cores KL49 (left) and KL51 (right) with positions of tephra layers.

proximal deposits (Fig. 6). A similar bimodal composition has been identified in a weathered ash deposit (M9-1) above the Vourvoulos tephra at Phira Steps, suggesting a tentative correlation of the CCT with the M9 Inter-Plinian interval (Fig. S1-14). Megalo Vouno scoriae are characterised by a slightly less silicic chemistry compared to the CCT (Fig. 6). Pumice layers intercalated in the Megalo Vouno cinder cone are bimodal (dacitic and rhyolitic) in composition. The dacitic component closely matches the Upper Scoriae 1 glass composition, while the silicic component is somewhat similar to the unknown rhyolitic one in the CCT (Figs. 6, S1-14). The age of the MV cinder cone has been roughly established by K/Ar dating between 54 ± 23 ka and 76 ± 28 ka (Druitt et al., 1999), and stratigraphic relationships suggested by Vespa et al. (2006) restrict it to between the Vourvoulos eruption and the formation of the Skaros Lava Shield (67 ± 9 ka; Fig. 2). This implies the MV deposits were erupted during either the M9 or early M10 Inter-Plinian intervals. Comparison of MV glass chemistries with the M9 Inter-Plinian units show no match (Fig. S1-14), leaving only the possibility of a correlation to the early M10a Inter-Plinian deposits (as proposed by Vespa et al., 2006). Indeed, the geochemical similarity of the intermediate component of the MV deposits to the US1 (Fig. S-14) implies that these two events may have been synchronous; a possibility which is supported further in chapter 6 by the composition of the X-1 tephra layer in deep-sea core KL49.

6. Marine tephra correlations

Proximal-marine tephra correlations used a combination of glass chemical matches and information on tephra grain size and chronostratigraphic position in the marine cores that are consistent with the proximal tephra record on Santorini (Druitt et al., 1999). Cores KL49 and KL51 were used to construct a composite tephrostratigraphic framework for the last ~200 kyrs southeast of Santorini. Core KL49 is the closest site to Santorini (30 km) and hence covers the last ~87 kyrs (MIS 1 to MIS 5a) of Santorini activity in greater detail than the distal cores LC21 and KL51. Glass compositions helped to identify 13 visible tephra layers in core KL49 that could be assigned to Plinian and Inter-Plinian Santorini eruptive events (Fig. 3, Table 2).

Core KL51 derived from the deepest and most distal site 250 km southeast of Santorini. Its sediments are characterised by lower accumulation rates compared to core KL49, and therefore, KL51 covers a larger time interval extending back to ~200 ka (MIS 7 – 1). Ten macroscopic visible tephra layers could be attributed to Santorini Plinian and Inter-Plinian activity based on the same criteria as KL49 tephras (Fig. 3, Table 2).

Core LC21 is located in an intermediate position ca. 130 km southeast of Santorini between sites KL49 and KL51 (Fig. 1). Core LC21 has the highest sediment accumulation rates of all three studied marine cores and extends back to ~160 ka (MIS 6 to MIS 1; Grant et al., 2012). Three visible and two cryptotephra layers of Santorini provenance have been identified, three of which have not been assigned to a specific eruptions yet (Satow et al., 2015). The visible Campanian Ignimbrite (39.9 ± 0.1 ka) in all three cores and the Kos Plateau Tuff (161.3 ± 1.1 ka; Smith et al., 1996) in KL51 and LC21 were used as chronostratigraphical markers to link the three tephra records and to build a reliable composite tephrostratigraphy (Fig. 3, Table 2).

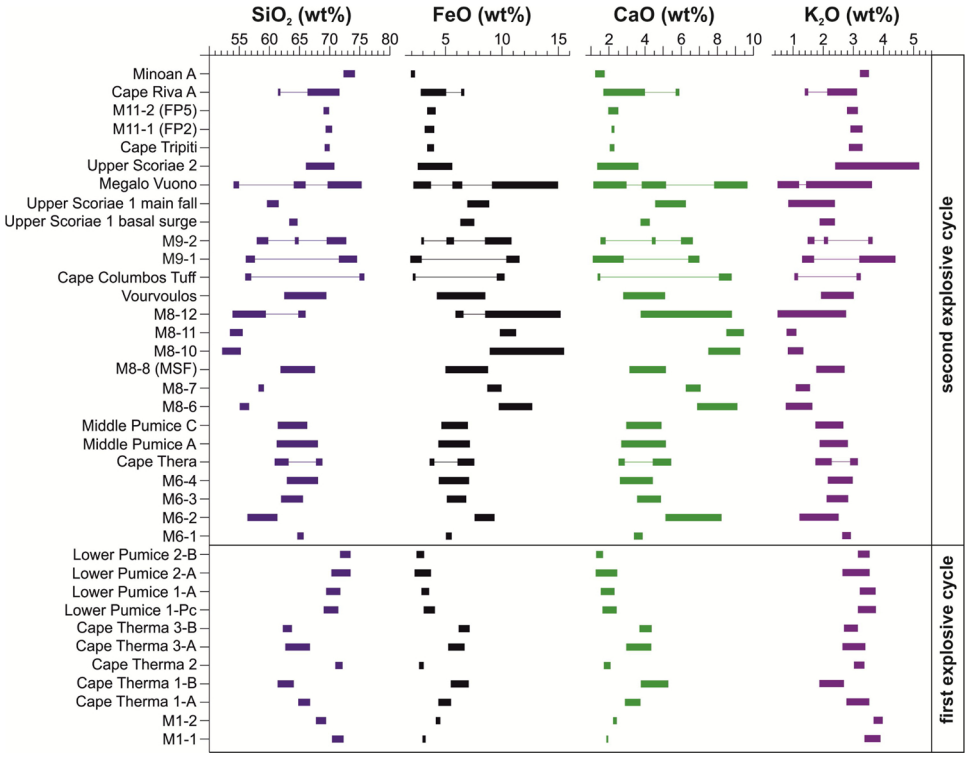

Fig. 6. Glass elemental variations in SiO_2, FeO, CaO and K_2O (data recalculated to 100 wt%, free of volatiles) of proximal tephra deposits listed in stratigraphic order (data from this study only).

In the following, proximal-marine correlations are discussed in stratigraphic order from the oldest to the youngest deposits.

6.1. KL51-639.5/Intra-S7 (Cape Therma 3)

The oldest marine tephra is a 2.5-cm-thick, fine-grained, dark grey ash layer that is recorded in core KL51 within sapropel S7. Interpolation of the KL51 chronology provided an age estimate for this tephra at 200.2 ± 0.9 ka (Table 2). KL51-639.5 glasses are characterised by a bimodal, andesitic to dacitic glass composition that overlaps with both CTM1 (A,B) and CTM3 (A,B) glass compositions of the new proximal dataset and best agrees with the CTM3-A glass data of Schwarz (2000) (Fig. 7 a). A correlation with the CTM3 eruption is also supported by the chronostratigraphic position of the KL51-639.5 tephra at ~200 ka, which is in agreement with the K/Ar age of CTM3 underlying Alonaki lavas at 224 ± 5 ka (Druitt et al., 1999); whereas correlation of the KL51-639.5/Intra-S7 tephra layer to the CTM1 eruption is contradicted by the much older age constraint of the proximal CTM1 deposits at ~360 ka (Druitt et al., 1999).

6.2. KL51-594/V-3 and KL51-591 (Lower Pumice 1 and M5 Inter-Plinian?)

Two tephra layers in core KL51 occur between sapropel S7 and S6 at 594 and 591 cm depth. The lowermost, 2-cm-thick ash layer KL51-594 is the equivalent of the marine V-3 tephra (Hieke et al., 1999) and occurs ~16 cm below sapropel S6. It is dated by sapropel interpolation in core KL51 at 185.7 ± 0.7 ka (Table 2). KL51-594/V-3 has a relatively homogenous rhyodacitic glass composition that best matches the major element chemistry of the proximal LP1-A fall deposits of both the new and the Schwarz (2000) dataset (Fig. 7b).

The V-3 tephra is closely succeeded by a 1-cm-thick horizon of light grey pumice-lapilli and fine-grained ash. Tephra KL51-591 shows a similar V-3 chemistry except for slightly higher FeO values, resembling the LP1-C (ignimbrite) average glass data by Druitt et al. (1999) (Fig. 7b), which suggests potential reworking of the underlying KL51-594/V-3 tephra. However, KL51-591 is deposited 1 cm above the V-3 tephra which indicates a considerable time span of several hundred years in between both layers; therefore, alternatively it could also be derived from a discrete unknown eruptive event within the M5 Inter-Plinian time interval that may have closely followed the LP1 eruption at 185.1 ± 0.7 ka (Fig. 2, Table 2). However, there is no evidence for volcanic activity between the LP1 and LP2 eruption in the proximal record, hence preventing the collection of glass chemical data for a more detailed comparison with the marine tephra data.

6.3. KL51-559.5/V-1 (Lower Pumice 2)

Further up-core in KL51, a 6-cm-thick, fine-grained, light greyish ash layer (KL51-559.5), previously related to the marine V-1 tephra (Hieke et al., 1999), occurs within sapropel S6. KL51-559.5/V-1 has a rhyolitic glass composition that best matches the composition of LP2-A pumices (Fig. 7b). The age of this marine tephra, and thus the LP2 eruption, is interpolated on the basis of the KL51 chronology to 176.7 ± 0.6 ka (Table 2). It is chronostratigraphically in agreement with the $^{40}Ar/^{39}Ar$ age of Simandiri lavas at 172 ± 4 ka which overly the proximal LP2 deposits (Druitt et al., 1999), additionally supporting a correlation of the V-1 tephra with the LP2 eruption.

6.4. KL51-498.5 and LC21-1119 (Cape Thera)

Approximately 12 cm above the Kos Plateau Tuff (~161 ka) in core KL51 is a 2-mm-thick, fine ash layer, KL51-498.5, which is dated by sapropel interpolation at 156.9 ± 2.3 ka (Table 2). KL51-498.5 has a heterogeneous andesitic to dacitic chemistry that approximates the composition of both CTA-A and CTA-B (mean) glasses and partly overlaps with MP glass compositions (Fig. 8 a). It is stratigraphically positioned below the marine W-2 (KL51-455) which is associated with the Middle Pumice eruption, hence in addition to the glass chemical trend a correlation with the Cape Thera eruption is proposed.

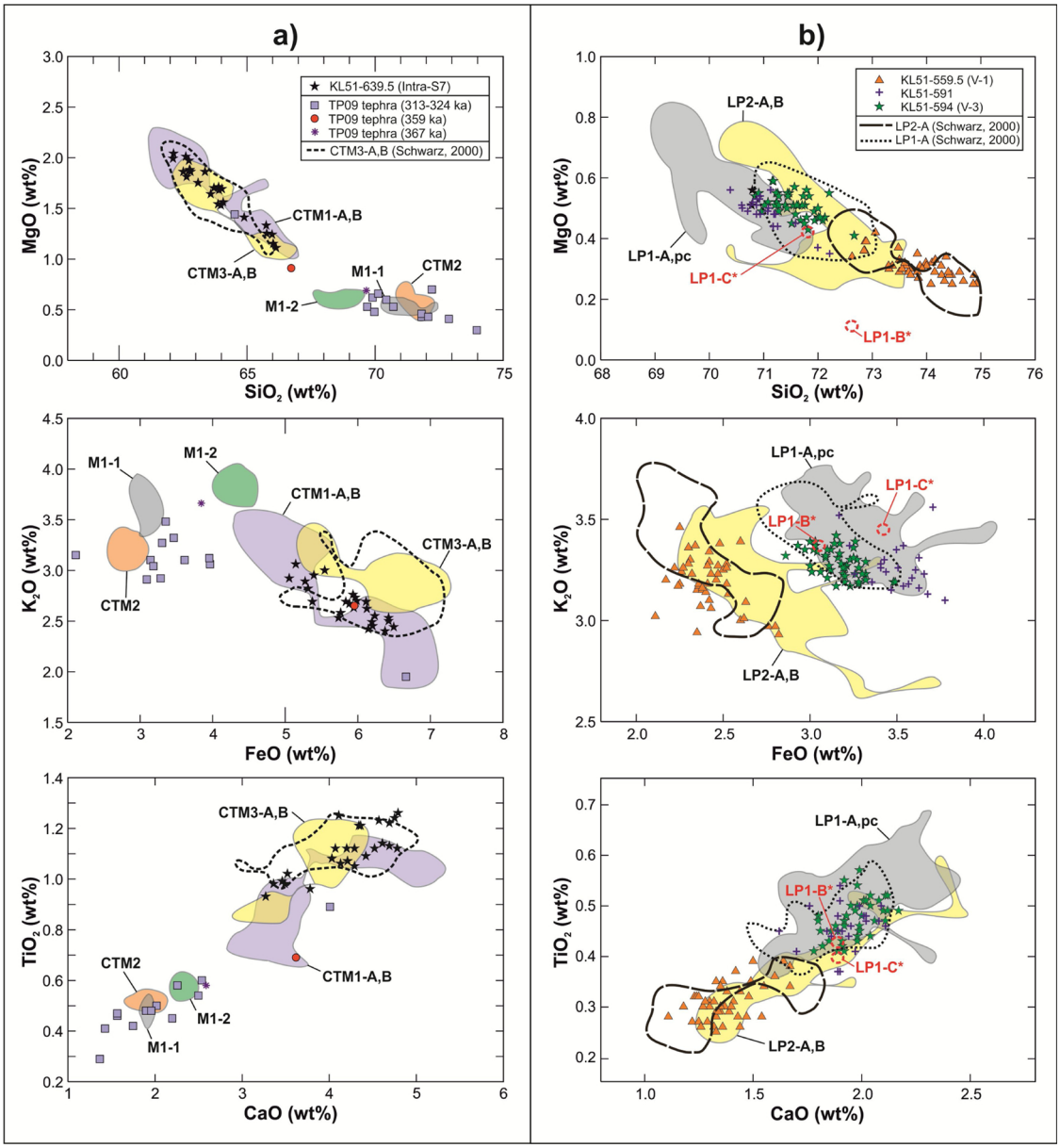

Fig. 7. Bivariate elemental plots of marine tephra glass data of core KL51 in comparison with proximal tephra data from **a)** the M1 to CTM3 interval (~360-200 ka) and **b)** the LP1 and LP2 eruptions (~190-170 ka). Proximal glass data derived from this study; data from Schwarz (2000) is indicated as black lines, and average EDS glass data from the LP1-B and LP1-C ignimbritic units are added as red dotted circles (*Druitt et al., 1999) (For interpretation of the references to colour in this figure legend, the reader is referred to the web version of this article.).

In core LC21, a massive, 42-cm-thick Santorini tephra, namely LC21-1119.0, occurs in a similar chronostratigraphic position above the KTP and is dated at 152.6 ± 9.3 ka (Satow et al., 2015). Only a few glass shards have been analysed in LC21-1119.0 (n = 6), and due to the high microlite content these show a scattered andesitic to dacitic composition that fall into the fields of both the CTA and MP compositions (Fig. 8a). Due to its similar age and chemical composition we propose a tentative correlation of LC21-1119.0 with tephra KL51-498.5 and the CTA eruption.

6.5. KL51-482 and KL51-466 (M7 Inter-Plinian?)

In core KL51, two discontinuous ash layers of several mm thickness occur above the KL51-498.5/CTA tephra at 482 cm (150.5 ± 2.4 ka) and 466 cm depth (144.3 ± 2.6 ka). The lowermost KL51-482 tephra has a similar andesitic-dacitic glass composition as KL51-498.5/CTA, while KL51-466 shows a distinct, homogeneous andesitic chemistry (Fig. 8a). Due to their stratigraphical position between the CTA and MP tephras, KL51-482 and KL51-466 most probably relate to M7 Inter-Plinian activity (Table 2), but due to the lack of proximal M7 glass data a precise assignment is not possible at this time.

6.6. KL51-455/W-2 (Middle Pumice)

In core KL51 between sapropel S6 and S5, a 2.5-cm-thick, relatively coarse lapilli layer occurs that has been previously assigned to the W-2 marine tephra (Hieke et al., 1999). Tephra KL51-455 has a heterogenic dacitic glass composition which matches best the composition of the Middle Pumice A fall deposits (Fig. 8a). It is dated by the KL51 chronology to 141.0 ± 2.6 ka (Table 2).

6.7. KL51-448 (M8 Inter-Plinian deposits, MSF?)

Approximately 5.5 cm above the KL51-455/W-2 tephra the coarse-grained (up to 5 mm diameter) and well-sorted (no ash) pumiceous

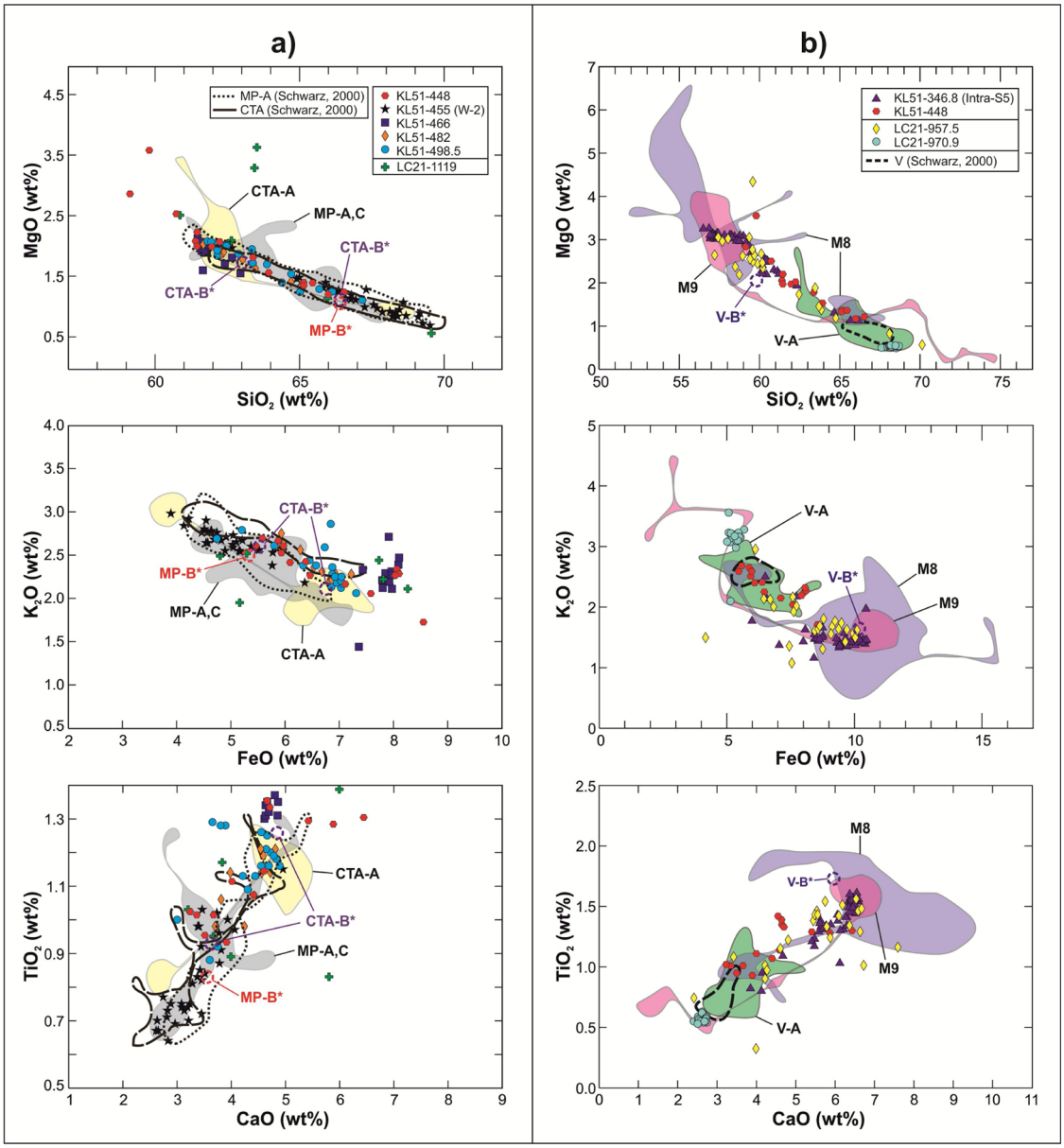

Fig. 8. Bivariate elemental plots of marine tephra glass data of cores KL51 and LC21 in comparison with proximal tephra data from **a)** the CTA to MP interval (~160-140 ka) and **b)** the M8, Vourvoulos and M9 eruptions (~140-100 ka). Proximal glass data derived from this study; data from Schwarz (2000) are indicated as black lines; average EDS glass data from *Druitt et al. (1999) is added for the CTA-B scoria flow (purple circles) and for the ignimbritic units MP-B (red circle) and V-B (blue circle) (For interpretation of the references to colour in this figure legend, the reader is referred to the web version of this article.).

lapilli layer KL51-448 appears. It is ~1 cm thick and has an interpolated age of 138.7 ± 2.7 ka (Table 2). The glass composition of KL51-448 is less-silicic than that of KL51-455 and approximates the andesitic-dacitic chemistry of the M8 Main Scoriae Fall (MSF) deposit of Vespa et al. (2006) (Fig. 8b).

6.8. LC21-970.9 (Vourvoulos), KL51-346.8/Intra-S5 and LC21-957.5 (M9 Inter-Plinian)

The well-laminated top part of sapropel S5 in core KL51 contains a 5-mm-thin, fine-grained ash layer at 346.8 cm depth (Schwarz, 2000; Moller et al., 2012). It is dated by linear interpolation between the upper (121.5 ka) and lower (128.3) sapropel boundary ages at 121.8 ± 2.9 ka. KL51-346.8/Intra-S5 is characterised by an andesitic glass composition that mainly overlaps with that of M9-2 Inter-Plinian deposits and partly falls within the fields of the Vourvoulos A fall and Vourvoulos B (co)ignimbritic deposits (Fig. 8b).

In core LC21, two tephra layers of Santorini provenance occur within sapropel S5 (Satow et al., 2015). The lower tephra is a visible 1-mm-thick layer, LC21-970.9, which shows a homogeneous dacitic-trachydacitic glass chemistry (Satow et al., 2015) that overlaps with the silicic end-member composition of the Vourvoulos A fall deposits (Fig. 8b). The age of 126.5 ± 2.9 ka for the LC21-970.9 tephra (Satow et al., 2015) is the first precise age to be derived for the Vourvoulos eruption. The other tephra sample within sapropel S5, LC21-957.5, is taken from a > 80 cm glass-shard-rich sediment package above the visible LC21-970.9 tephra (Satow et al., 2015). The base of this shard rich sediment package is separated from the LC21-970.9 tephra by about 10 cm of tephra-free pelagic sediments, implying that it was deposited a significant time after the Vourvoulos eruption. Notably, sample LC21-957.5 has a heterogeneous andesitic to minor dacitic glass composition that fully matches the composition of the visible KL51-346.8/Intra-S5 tephra in core KL51 (Fig. 8b), and hence the two tephra layers are likely to relate to the same eruptive event. Despite the need for further sedimentological

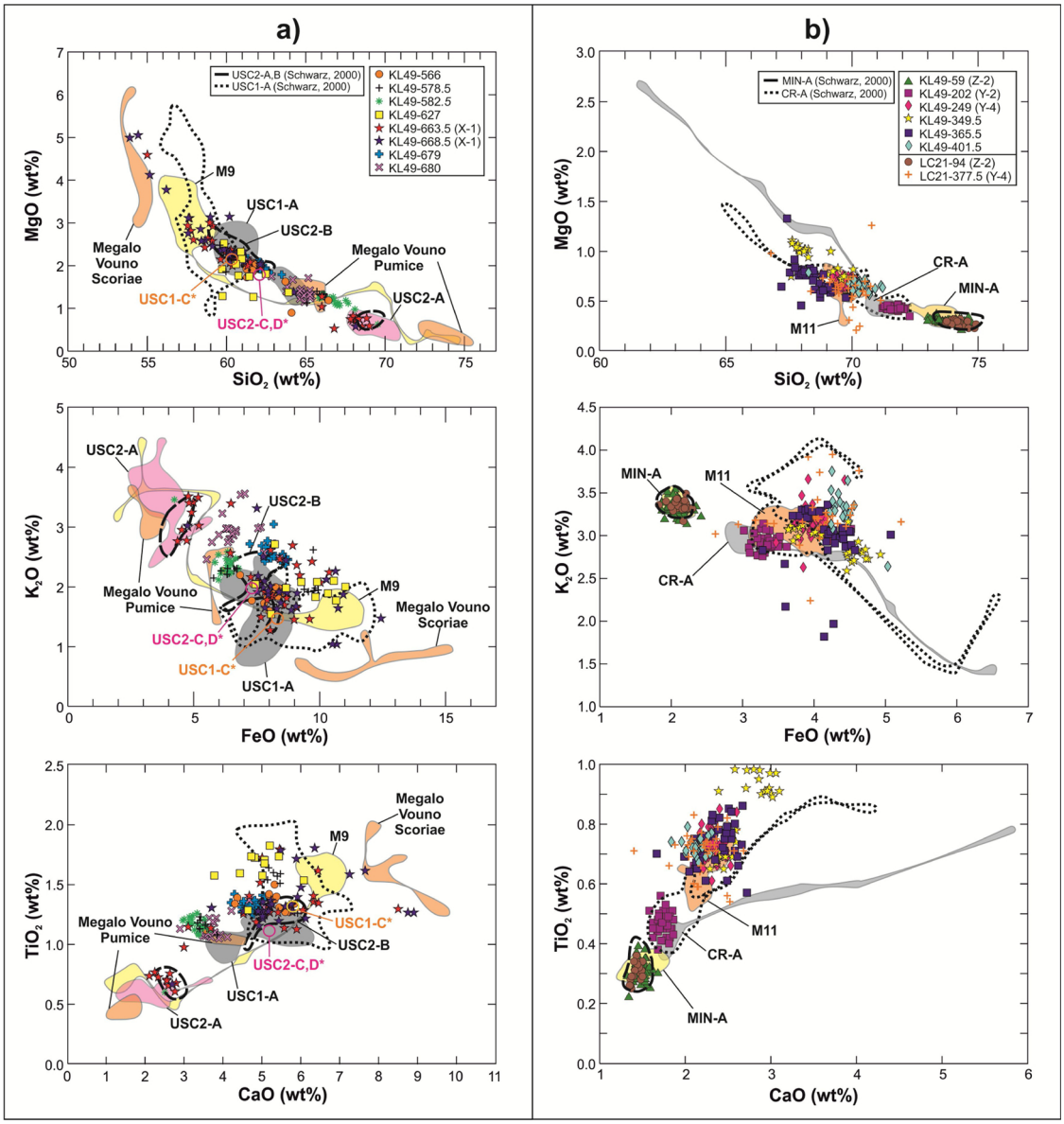

Fig. 9. Bivariate elemental plots of marine tephra glass data of cores KL51 and LC21 in comparison with proximal tephra data from **a)** the M9 to USC2 interval (~100-50 ka) and **b)** the M11b, Cape Riva and Minoan eruptions (~50-3.6 ka). Proximal glass data derived from this study; data from Schwarz (2000) are indicated as black lines. Average EDS glass data from *Druitt et al. (1999) for scoria flows USC1-C (orange circle) and USC2-C,D (pink circles) have been added for complementing the proximal dataset (For interpretation of the references to colour in this figure legend, the reader is referred to the web version of this article.).

investigations of core LC21, we propose a tentative correlation of both the LC21-957.5 and KL51-346.8/Intra-S5 tephra layers to M9 Inter-Plinian deposits. This is supported by their stratigraphic position just above the Vourvoulos tephra (LC21-970.9) and overlapping geochemical composition with the proximal M9 deposits (Figs. 8b and S1-14). M9-2 scoria deposits, with a slightly lower FeO content than the M9-1 weathered ash, are the best match to LC21-957.5 and KL51-346.8/Intra-S5. The interpolated age for this event derives from the KL51 chronology and is defined at 121.8 ± 2.9 ka (Table 2).

6.9. KL49-680 and KL49-679 (USC1 precursory?)

The oldest tephra layers in core KL49 are two 1–2-mm-thin, fine-grained black ash layers, namely KL49-680 and KL49-679, that both occur within the lower part of sapropel S3. The older tephra KL49-680, dated at 83.8 ± 2.9 ka, is characterised by a dacitic to minor trachy-dacitic glass composition, which resembles both the composition of the pumice clasts within the basal surge deposits of the USC1 eruption and of the minor dacitic component of the Megalo Vouno pumices (Fig. 9 a). The younger KL49-679 tephra (83.5 ± 2.9 ka) has a distinct andesitic composition that approximates more closely the USC1-A main fall composition (Fig. 9a). However, small grain sizes and low thicknesses of both layers in the most proximal core KL49 indicate relatively low-energetic eruption dynamics; hence, we suggest a correlation with fall and flow units that were deposited prior to the main andesitic USC1-A fall tephra, which itself is deposited ~3 cm further upcore in core KL49.

6.10. KL49-668.5/X-1 (Upper Scoriae 1, Megalo Vouno and Upper Scoriae 2?)

The most prominent tephra in core KL49 is the 8.5-cm-thick, coarse-grained KL49-668.5 tephra, which has been previously related to the marine X-1 tephra (Hieke et al., 1999; Schwarz, 2000). It occurs directly on top of sapropel S3 and hence is dated by the KL49 age model at 80.8 ± 2.9 ka (Table 2). Notably, the KL49-668.5/X-1 tephra is sub-divided into two sublayers. The lower, 5-cm-thick layer is a black-

Table 2
Summary of ages and glass geochemistries of Plinian (in bold) and Inter-Plinian Santorini eruptive events and their attribution to primary distal marine correlatives. Well-dated tephra layers from Italy (Y-5) and Kos (W-3) are also included as chronostratigraphic information. BA = basaltic andesitic, A = andesitic, TrA = trachyandesitic, D = dacitic, TrD = trachydacitic, RD = rhyodacitic, R = rhyolitic.

Eruption	Glass geochemistry	Core depth KL49 (cm)	Core depth LC21 (cm)	Core depth KL51 (cm)	Age (cal a BP) with 2σ uncertainty	Age reference
Minoan	R	15-59 (Z-2)	71.6-94.0 (Z-2)	–	3563 ± 13	Friedrich et al. (2006)
Cape Riva	R	172.5-202 (Y-2)	–	–	22,024 ± 642	Bronk Ramsey et al. (2015)
M11b (Cape Tripiti?)	D-RD	242-249 (Y-4)	377.5 (Y-4)	–	27,480 ± 1440	Satow et al. (2015)
Campanian Ignimbrite	Tr-P	344-349.5 (Y-5)	479.5-492.5 (Y-5)	90-92.5 (Y-5)	39,850 ± 140	Giaccio et al. (2017b)
+ M11b (2 events)?	D, RD		–	–		
M11b?	RD-TrD	362-365.5	–	–	41,620 ± 260	This study
M11b?	RD-(TrD)	400-401.5	–	–	46,520 ± 590	This study
M11a?	A-D	564-566	–	–	69,590 ± 2140	This study
M11a (2 events)?	D, A	572-578.5	–	–	70,440 ± 2200	This study
M11a?	D	580.5-582.5	–	–	70,720 ± 2220	This study
M11a?	A	623-627	–	–	76,470 ± 2610	This study
Upper Scoriae 2?	A, D	660-663.5 (X-1)			?	
Upper Scoriae 1	A	663.5-668.5 (X-1)	–	–	80,800 ± 2900	This study
+ Megalo Vouno?	+ BA		–	–		
USC1 precursory?	A	679 (Intra-S3)	–	–	83,540 ± 2900	This study
USC1 precursory?	D-TrD	680 (Intra-S3)	–	–	83,800 ± 2900	This study
M9-2	A-BA	–	957.5	346.8 (Intra-S5)	121,830 ± 2900	This study
Vourvoulos	D-TrD	–	970.9	–	126,510 ± 2920	Satow et al. (2015)
M8-8 (MSF)?	A-D	–	–	447-448 cm	138,720 ± 2680	This study
Middle Pumice	A-D	–	–	452.5-455 cm (W-2)	141,040 ± 2630	This study
M7?	A	–	–	466 cm	144,320 ± 2560	This study
M7?	A-D	–	–	482 cm	150,490 ± 2430	
Cape Thera	A-D	–	1077-1119 (?)	498.5 cm	156,860 ± 2290	This study
					152,590 ± 9320	Satow et al. (2015)
Kos Plateau Tuff	High-silica R	–	1234.5-1246.5	507-510 (W-3)	161,300 ± 2200	Smith et al. (1996)
Lower Pumice 2	R	–	–	553-559.5 (V-1)	176,700 ± 590	This study
M5?	R-RD	–	–	590-591	185,080 ± 710	This study
Lower Pumice 1	R-RD	–	–	592-594 (V-3)	185,740 ± 720	This study
Cape Therma 3	TrA/A-TrD/D	–	–	637-639.5 (Intra-S7)	200,210 ± 880	This study

greyish, coarse-grained (up to 3 cm diameter) scoria lapilli deposit that is characterised by a heterogeneous andesitic-dacitic and basaltic andesitic composition (Fig. 9a). The majority of the intermediate glasses correlate well with the USC1 fall and flow deposits, while the minor mafic components approximate the glass composition of the Megalo Vouno Scoriae (Fig. 9a), hinting at the possibility of a synchronous eruption of this cinder cone at the time of the USC1 eruption.

The upper part of the X-1 tephra is a much more fine-grained, black sand layer. Its glasses show a bimodal andesitic and dacitic composition that correlates best with the proximal USC2-A pumice fall and USC2-B scoria flows chemistries (Fig. 9a). Schwarz (2000) reports other X-1 tephra occurrences in more distal marine cores south of Crete where this tephra occurs as a double layer above sapropel S3. Although glass chemical data are not available, the two distinct X-1 layers are a strong indication for two separate, closely-spaced major eruptive events around 70–80 ka. Low sedimentation rates and/or submarine erosional processes at the site of core KL49 could have led to a compression of several tephra events including a large number (n = 30) of M10 Inter-Plinian units as described by Vespa et al. (2006), supporting the idea that the X-1 tephra could potentially represent both the USC1 and USC2 eruptions. However, this is rather speculative and requires sedimentological evidence from core KL49. Consequently, other distal marine or terrestrial sediment archives need to be studied to resolve the tephrostratigraphical framework for this particular time interval.

6.11. KL49-627, KL49-582.5, KL49-578.5 and KL49-566 (M11a Inter-Plinian)

The KL49-668.5/X-1 tephra is overlain by a succession of four dark, fine-grained ash layers that are dated by interpolation between ~77 ka and 69 ka (Table 2). The lowermost tephra KL49-627 (76.5 ± 2.6 ka) is made up of three closely-spaced, blackish-brown ash lenses in 623, 624 and 627 cm depth. Their glass chemistry is identical andesitic and resembles the composition of the proximal USC2-B deposit except for slightly lower MgO and higher TiO_2 concentrations (Fig. 9a). The overlying tephra KL49-582.5 (70.7 ± 2.2 ka) is a 2-cm-thick, disperse ash layer with a distinct dacitic glass composition that plots between the USC2-A and USC2-B fields (Fig. 9a). It is closely succeeded by the 6.5-cm-thick, disperse KL49-578.5 tephra (70.4 ± 2.2 ka), which is bimodal in composition and overlaps with the andesitic KL49-627 and dacitic KL49-582.5 chemistries (Fig. 9a). It likely represents two compositionally different but synchronous eruptive events. The uppermost layer KL49-566, dated at 69.6 ± 2.1 ka, is a 2-cm-thick, dark ash with diffuse lower and upper boundaries. It has a mainly andesitic to minor dacitic glass composition that resembles the andesitic chemistry of the KL49-627 and KL578.5 tephras except for slightly lower FeO and TiO_2 concentrations (Fig. 9a).

Because of the fine-grained nature of tephra components and the glass chemical affinities to the USC2 deposits, the four ash layers in core KL49 may correlate with early M11a Inter-Plinian activity that directly followed the USC2 eruption. Vespa et al. (2006) report six major M11a Inter-Plinian eruption units in the proximal record on Santorini that are characterised by intermediate bulk compositions. Five of these units could be related to the KL49 tephras; however, proximal glass chemistries are still required for potentially confirming and detailing these attributions.

6.12. KL49-401.5, KL49-365.5 and KL49-349.5 (M11b Inter-Plinian)

The MIS 3 interval of core KL49 between ~47 ka and 39 ka comprises three visible tephra layers of distinct rhyodacitic glass compositions (Table 2). The lowermost tephra KL49-401.5 is a few millimetres thick lens of fine-grained, beige ash that is dated at 46.5 ± 0.7 ka. It has the most evolved glass chemistry with ~67-72 wt% SiO_2 and approximates the composition of both the proximal USC2-A pumice fall

and the M11b Inter-Plinian deposits (Fig. 9b). Tephra KL49-365.5 (41.6 ± 0.4 ka) is a 3.5-cm-thick, dark greyish-brown ash layer that has a slightly less silicic glass composition (~67-70 wt% SiO_2) with higher CaO and lower K_2O concentration compared to the preceding KL49-401.5 tephra (Fig. 9b). The uppermost tephra KL49-349.5 is a 5.5-cm-thick, brownish grey, poorly sorted pumice-lapilli and ash deposit that comprises three different glass compositions. The dominant component is dacitic with ~67-69 wt% SiO_2. The second main glass population is a rhyodacite that overlaps with the chemistry of the Y-4 tephra that occurs further upcore (Fig. 9b). KL49-349.5 contains also a minor phonolitic-trachytic glass component that correlates well with the Campanian Ignimbrite, hence dating the tephra at 39.9 ± 0.1 ka (Fig. 5). The Campanian Ignimbrite (or marine Y-5 tephra) occurs also as visible layer in cores LC21 (Satow et al., 2015) and KL51 and therefore forms a valuable isochron for linking the three cores (Fig. 3).

6.13. KL49-249/Y-4 and LC21-377.5 (Cape Tripiti?)

Tephra KL49-249 occurs in the lower part of the MIS 2 interval in core KL49 and is a ca. 7-cm-thick, dark brownish violet ash layer. It has a homogenous rhyodacitic glass composition that agrees well with the major element chemistry of the marine LC21-377.5/Y-4 cryptotephra in core LC21 (Fig. 9b), where it is dated at 27.5 ± 1.4 ka BP (Satow et al., 2015). Schwarz (2000) originally proposed an assignment of Y-4 to the Upper Scoriae 2 eruption, which was revised by Fabbro et al. (2013) who correlated averaged Y-4 data from core KL49 (Schwarz, 2000) and other Aegean Sea cores (Vinci, 1985) with the Cape Tripiti Pumice. The more detailed comparison of the whole KL49-249/Y-4 dataset with new proximal glass data from the Cape Tripiti Pumice, M11-1/FP2, and M11-2/FP5 pyroclastic units confirms an assignment to Santorini M11b activity but does not allow a clear assignment to any of the three units (Fig. 9b).

6.14. KL49-202/Y-2 (Cape Riva)

The most prominent tephra within the late MIS 2 interval is the ca. 29.5-cm-thick KL49-202 layer that is located ca. 80 cm below sapropel S1. It consists of light greyish brown, fine lapilli to sandy stratified material. KL49-202 has a rhyolitic major element chemistry that best matches the composition of both the marine Y-2 tephra and the proximal CR-A fall deposits dated at 22.0 ± 0.6 ka (2σ uncertainty; Bronk Ramsey et al., 2015) (Fig. 9b). This correlation is in agreement with previous interpretations (Schwarz, 2000; Wulf et al., 2002).

6.15. KL49-59/Z-2 and LC21-94 (Minoan)

Tephra KL49-59 is positioned above sapropel S1 and represents the youngest and most prominent tephra in core KL49. It is a 44-cm-thick, pale greyish-brown pumice-lapilli (up to 3 cm diameter) deposit that is stratified with pale fine lapilli and darker sandy layers. The rhyolitic glass composition clearly assigns KL49-59 to the marine Z-2 and proximal Minoan tephra dated at ~3.6 ka (Friedrich et al., 2006) (Fig. 9b). It also correlates with tephra LC21-94 in the more distal core LC21, where it forms a 23-cm thick ash layer (Satow et al., 2015).

7. Constraining Santorini eruption ages

7.1. Ages of marine distal tephras

The different temporal ranges of the three Aegean Sea cores KL49, KL51 and LC21 allowed the preservation of Santorini tephra events from different, partly overlapping time intervals (Table 2). Using mutual prominent tephra markers, such as the Campanian Ignimbrite (all three cores) at 39.9 ± 0.1 ka and the Kos Plateau Tuff (cores KL51 and LC21) at 161.3 ± 2.2 ka, facilitates the construction of a continuous distal Santorini tephrostratigraphic framework that covers the last ~200 kyrs (Fig. 3, Table 1).

As a result, the newly compiled marine tephrostratigraphy encompasses 27 single eruptive events from Santorini, including ten Plinian and 17 Inter-Plinian eruptions (Table 2). The new age models of cores KL49 and KL51 (this study) as well as the high-resolution LC21 chronology (Grant et al., 2012, 2016; Satow et al., 2015) enabled new and/or higher precision dating of previously non- or poorly dated Santorini Plinian events. For example, new eruption dates have been determined for the Vourvoulos (126.5 ± 2.9 ka) and Cape Thera (156.9 ± 2.3 ka) eruptions. Furthermore, the new KL49 and KL51 chronologies have updated the age models provided by Keller et al. (2000) and hence now provide higher-precision ages for the Upper Scoriae 1 (80.8 ± 2.9 ka), Middle Pumice (141.0 ± 2.6 ka), Lower Pumice 2 (176.7 ± 0.6 ka), Lower Pumice 1 (185.7 ± 0.7 ka), and Cape Therma 3 eruptions (200.2 ± 0.9 ka).

Attaining a reliable age estimation of the Upper Scoriae 2 eruption was problematic due the difficulty in unambiguously identifying this tephra as a separate layer in core KL49; its possible stratigraphic position is within the prominent X-1 tephra directly above the USC1 layer. This in addition to rather vague information about its chronostratigraphical position within the X-1 double layers in other distal cores (Schwarz, 2000) only allows for constraining a maximum age of the USC2 eruption at 80.8 ± 2.9 ka (the date of the Upper Scoriae 1). In the proximal record, the $^{40}Ar/^{39}Ar$ (whole rock) age of the underlying Skaros lavas at 67 ± 9 ka (1σ) provides another maximum age for the USC2 eruption, which lies within the 2σ error range of the marine age estimate. A more reliable $^{40}Ar/^{39}Ar$ groundmass age of a lava flow that overlies the USC2 deposits at Therasia (48.2 ± 2.4 ka) was derived by Fabbro et al. (2013). This lava is separated from the USC2 deposits by a well-developed palaeosol and represents a minimum age for the USC2 eruption (Fabbro et al., 2013). Direct radioisotopic dating on whole rock material of the USC2 fall deposits has defined its eruption age as either 79 ± 8 ka (1σ, mean K/Ar age) or 54.0 ± 3.0 ka (1σ, $^{40}Ar/^{39}Ar$) (Druitt et al., 1999). The latter $^{40}Ar/^{39}Ar$ date is considered to be the most accurate one at this time as this is a plateau date which should account for any influence from excess argon. It is furthermore also chronostratigraphically in accordance with the date of 67 ± 9 ka (1σ; Druitt et al., 1999) defined for the underlying Skaros lava shield. However, the KL49 marine record indicates that the USC2 eruption is probably older than 54 ka since it closely followed the USC1 event at 80.8 ± 2.9 ka. Only further tephra studies in other distal marine and terrestrial sites as well as new direct dating with modern and more reliable techniques can solve the USC2 dating issue.

The marine tephra records also allow for the identification and first dating of Inter-Plinian Santorini activity. The KL49 site nearest to Santorini, for instance, records eruptions preceding USC1 from the M9 interval at 83.8 and 83.5 ± 2.9 ka. KL49 also documents at least ten eruptive events from the M11 Inter-Plinian interval. Those are clustered within two time intervals between 76.5 ± 2.6 ka and 69.6 ± 2.2 ka (M11a; n = 5) and between 46.5 ± 0.6 ka and 27.5 ± 1.4 ka (M11b; n = 5), respectively.

The previously proposed stratigraphic positions of the Megalo Vouno (MV) cinder cone within the early M10a sub-interval (Vespa et al., 2006) is supported by the detection of MV scoriae for the first time at a distal site. Its occurrence within the lower part of the X-1 tephra in core KL49 indicates formation of this cinder cone at around the time of the USC1 eruption (80.8 ± 2.9 ka). The proximal-terrestrial record, where thin dacitic pumice layers matching the USC1 composition are intercalated within the Megalo Vouno scoria, also suggests likely synchronous activity. Furthermore, the tentative assignment of the Cape Columbos Tuff with the proximal M9-1 weathered ash unit directly above the Vourvoulos deposit and the interpolated age estimate of overlying M9-2 scoriae (marine-terrestrial correlations) allow this tuff cone to be constrained to an age between 126.5 ± 2.9 ka and 121.8 ± 2.9 ka. This age is in good agreement with the previously proposed date of the Cape Columbos Tuff during a higher sea-level during MIS 5e that is similar to the present-day sea-level (Druitt et al.,

1999).

Older Inter-Plinian eruptions are documented in core KL51 only. Those include the M8 Main Scoriae Fall (MSF) deposit (Vespa et al., 2006) which occurs stratigraphically above the W-2 (Middle Pumice) deposit and is dated at 138.7 ± 2.7 ka. M7 Inter-Plinian activity between the Cape Thera and Middle Pumice eruptions is represented by at least two thin, geochemically slightly distinct fall deposits that are dated at 144.3 ± 2.6 ka and 150.5 ± 2.4 ka, respectively. The oldest Inter-Plinian deposits in the KL51 core potentially relate to the M5 interval and postdate the Lower Pumice 1 tephra to 185.1 ± 0.7 ka (Fig. 3, Table 1).

7.2. Palynostratigraphic age constrains of terrestrial distal tephras

The terrestrial peat record of Tenaghi Philippon (TP) in NE Greece (Pross et al., 2015) contains several cryptotephra layers in the MIS 11 to MIS 9 interval that can be connected to the initial phase of the first explosive cycle of Santorini activity (Vakhrameeva et al., 2018, 2019) (Fig. 2). The tephrostratigraphic record from TP is used here to complement the marine distal Santorini tephra record and to provide eruption age estimates for the older time interval (> 300 ka) of the first explosive cycle by palynostratigraphic dating (Vakhrameeva et al., 2018, 2019) (Fig. 2). Accordingly, the oldest Santorini tephra in the TP record occurs within the late MIS 11 interglacial at ~367 ka and is correlated with the M1-2 Inter-Plinian eruption (Vakhrameeva et al., 2018). It is followed by the Cape Therma 1 tephra at ~359 ka, placing this Plinian eruption at the transition of MIS 11 to MIS 10 (Vakhrameeva et al., 2018). Another eight cryptotephra layers of Santorini provenance form a cluster within the early MIS 9 interglacial and are dated palynostratigraphically between ~324 ka and 313 ka (Vakhrameeva et al., 2019). The heterogeneous rhyolitic compositions of these tephras approximate the glass composition of both the Cape Therma 2 and M1 tephras (Fig. 5). Based on their position above the CTM1 tephra, these layers are tentatively associated with yet unknown Santorini M2 Inter-Plinian activity (see detailed discussion in Vakhrameeva et al., 2019).

8. Santorini tephra dispersal

This study provides new insights into the south-easterly dispersal fan of Santorini tephras in a 250-km-long transect represented by the locations of the three marine cores KL49 (30 km distance to Santorini), LC21 (130 km) and KL51 (250 km) (Fig. 1). Although the low number of study sites precludes the generation of detailed isopach maps, tentative information on distribution patterns can be inferred for major tephras in combination with available published data (Table 3).

Santorini eruptions that have been long identified at distal marine sites in the Eastern Mediterranean region encompass the tephras V-3/LP1, V-1/LP2, W-2/MP, X-1/USC1-USC2, Y-2/CR, Y-4/Cape Tripiti, and Z-2/MIN (e.g., Keller et al., 1978; Federman and Carey, 1980; Keller, 1981; McCoy, 1981; Vinci, 1985). These tephras have relatively well defined tephra dispersal fans (McCoy, 1981), which, however, are limited to visible tephra findings only. Re-evaluation of these distribution patterns now also includes first cryptotephra findings and terrestrial tephra data (Fig. 10). Findings of older Santorini tephras include mainly the relatively thick MIS 6 layers V-3/LP1 (185.7 ± 0.7 ka), V-1/LP2 (176.7 ± 0.6 ka) and W-2/MP (141.0 ± 2.6 ka), which are restricted to core KL51 and to other sediment cores retrieved from deep-sea regions south of Crete, i.e., from the Levantine and Libyan Seas (McCoy, 1981; Vinci, 1985) (Fig. 10a). The apparent absence of these tephras north of Santorini is mainly because existing cores from the central and northern Aegean Sea exhibit relatively high sediment accumulation rates and hence do not extend as far back in time. Furthermore, evolving longer (crypto)tephrostratigraphies from distal terrestrial sites north of Santorini (e.g., Tenaghi Philippon; compare Pross et al., 2015; Wulf et al., 2018) still lack information from this particular time interval, and the few data available for the MIS 9 to MIS 11 cryptotephra record are restricted to the Tenaghi Philippon site only (Vakhrameeva et al., 2018, 2019). Sparse information for older Santorini tephras from the proximal-medial record (Druitt et al., 1999) make it particularly difficult to estimate preferred distribution patterns for these tephras.

Findings of the V-3/LP1 tephra have been reported in the Libyan and Levantine Basin but also further west in the Ionian Sea (Keller et al., 1978; McCoy, 1981) (Fig. 10a). However, Ionian Sea findings are not yet confirmed by glass geochemical data and hence have to be treated carefully. The W-2/MP tephra (141.0 ± 2.6 ka), on the other hand, has been only identified in the SE Aegean and Levantine Seas, confirming a main southerly to south-easterly dispersal direction of this tephra as proposed by proximal-medial findings (Druitt et al., 1999) (Fig. 10a).

The source and dispersal of the marine X-1 tephra (within MIS 5a) have long been controversial. The X-1 tephra has been found in similar stratigraphic positions above sapropel S3 in several cores from the Ionian, Libyan and Aegean Seas (Fig. 10b), and was linked to a mutual source from either Aeolian or Aegean Arc volcanoes (e.g., Federman and Carey, 1980; Keller, 1981; Keller et al., 1978; McCoy, 1981; Vinci, 1985). However, new EPMA glass data have evidenced that there are two different sources involved: The original X-1 tephra, found in Ionian Sea cores a few centimetres above S3 (Kraml, 1997), correlates well with tephra TM-21 in Lago Grande di Monticchio in southern Italy (Wulf et al., 2004). Both tephras have been correlated with the "Petrazza Tuffs" from Stromboli, Aeolian Islands, and dated at 75.3 ± 3.0 ka (Kraml, 1997; Wulf et al., 2004). Because of its distinct trachyandesitic to trachydacitic chemistry and its younger age, the former X-1 tephra in Ionian Sea cores has been relabelled as marine Y-9 tephra (Kraml, 1997; Wulf et al., 2004) (Table 3). The former X-1 (double) tephra detected in Aegean Sea cores, in turn, directly overlies S3 at 80.8 ± 2.9 ka and is correlated with the andesitic-dacitic USC1-USC2 eruptions of Santorini (Keller et al., 2000; Schwarz, 2000; this study). In this study, X-1 has been only identified in core KL49. Other distal X-1 findings include cores from the eastern-central Aegean Sea ca. 200 km NNE of Santorini (Aksu et al., 2008), as well as northwest (Vinci, 1985) and up to 300 km south of Crete (McCoy, 1981), the latter confirming a proposed southerly dispersal from the proximal-medial record (Druitt et al., 1999) (Fig. 10b).

Dispersal patterns of MIS 2 tephras Y-4, Y-2 and Z-2 are shown in Fig. 10c. All three tephras occur in cores KL49 and LC21, with only LC21 lacking the Y-2 tephra. The Y-4/Cape Tripiti? tephra (27.5 ± 1.1 ka) has the most limited distribution within the SE Aegean Sea (Aksu et al., 2008; Satow et al., 2015; this study), probably because of its relative weak eruptive nature. The Y-2/Cape Riva (22.0 ± 0.6 cal ka BP) and Z-2/Minoan tephras (3.6 cal ka BP), on the other hand, show a very widespread dispersal towards the East and North (Y-2) and the Northeast (Z-2) with main occurrences in the Levantine, Aegean and Black Seas (Fig. 10c).

Distribution patterns of other major Santorini tephras such as Intra-S7/Cape Therma 3, Cape Thera, and Intra-S5/M9-2 and Vourvoulos are difficult to reconstruct due to their single, first time findings in marine-distal cores (this study) and lack of information from the proximal-medial record. The Intra-S7/CTM3 (200.2 ± 0.9 ka) tephra, for instance, only occurs in core KL51 but is a relative thick layer in that core suggesting a likely south-easterly dispersal. Distal tephra from the Cape Thera (156.9 ± 2.3 ka, MIS 6) and Vourvoulos (126.5 ± 2.9 ka, MIS 5e) eruptions, in turn, are recorded in cores KL51 and LC21, respectively, only as very thin visible layers, indicating either weaker dynamics of these eruptions or a more southerly distribution compared to the Intra-S7/CTM3 tephra.

Newly detected distal tephras from minor, Inter-Plinian eruptions, i.e., eruptions from intervals M5, M7, M8, M9, M10, and M11 (Table 2), in the SE sector of Santorini suggest similar southerly to easterly dispersal patterns, however, these need to be tested by further findings.

Table 3
Revised Eastern Mediterranean marine tephrostratigraphy for the past 200 kyrs.

Tephra	Volcanic centre	Eruptive event	Dispersal	Age (ka)	Dating method	Age reference
Z-1	Somma-Vesuvius	Pompeii	SSE	AD79	Historical record	Lirer et al. (1973)
Z-2	Santorini	Minoan	E	3.6	^{14}C	Friedrich et al. (2006)
Z-3 to Z-5	Central Anatolia?	unknown	S	8-10	interpolated	McCoy (1981)
Y-1	Mount Etna	Biancavilla Ignimbrite	E	17.3 ± 0.4	^{14}C	Albert et al. (2013)
Y-2	Santorini	Cape Riva	N	22.0 ± 0.6	^{14}C	Bronk Ramsey et al. (2015)
Y-4	Santorini	Cape Tripiti/M11	SE	27.5 ± 1.4	interpolated (LC21)	Satow et al. (2015)
Y-3	Campi Flegrei	unknown	ESE	29.0 ± 0.4	^{14}C	Albert et al. (2015)
Y-5	Campi Flegrei	Campanian Ignimbrite	E	39.9 ± 0.1	^{40}Ar/^{39}Ar	Giaccio et al. (2017b)
Y-6	Pantelleria	Green Tuffs	E	45.7 ± 1.0	^{40}Ar/^{39}Ar	Scaillet et al. (2013)
Y-7	Ischia	Tufo Verde di Epomeo	SE	55.0 ± 2.0	^{40}Ar/^{39}Ar	Watts et al. (1996)
Y-8	Salina	Grey Porri Tuffs	SE	66.7 ± 2.0	interpolated	Kraml (1997)
Y-9 (former X-1)	Stromboli	Petrazza Tuffs	ENE	75.3 ± 2.0	interpolated	Kraml (1997)
X-1	Santorini	Upper Scoriae 1	S	80.8 ± 2.9	interpolated (KL49)	This study
X-4	Mount Etna	Acireale	E	89.5 ± 2.0	interpolated	Kraml (1997)
X-5	Campanian Province	Unknown	SE	106.2 ± 1.6	^{40}Ar/^{39}Ar	Giaccio et al. (2012)
X-6	Campanian Province	Unknown	E	109.5 ± 0.9	^{40}Ar/^{39}Ar	Regattieri et al. (2017)
W-0 (P-11)	Pantelleria	Ignimbrite P	E	133.5 ± 2.0	interpolated (LC21)	Satow et al. (2015)
W-1	Vico	Ignimbrite D	E	138.0 ± 2.0	K/Ar	Laurenzi and Villa (1987)
W-2	Santorini	Middle Pumice	S	141.0 ± 2.6	interpolated (KL51)	This study
W-3	Kos	Kos Plateau Tuff	S	161.3 ± 2.2	^{40}Ar/^{39}Ar	Smith et al. (1996)
V-0	Pantelleria	Ignimbrite S	E	171.0 ± 1.7	^{40}Ar/^{39}Ar	Rotolo et al. (2013)
V-1	Santorini	Lower Pumice 2	SE/SW	176.7 ± 0.6	interpolated (KL51)	This study
V-2	Roman Province	Unknown	SE	176.9 ± 2.0	interpolated	Kraml (1997)
V-3	Santorini	Lower Pumice 1	SE/SW	185.7 ± 0.7	interpolated (KL51)	This study
Intra-S7	Santorini	Cape Therma 3	SE?	200.2 ± 0.9	interpolated (KL51)	This study

9. Concluding remarks and perspectives for future research

This study presents an expanded compilation of glass geochemical data (> 1000 analyses) for all Plinian and numerous Inter-Plinian proximal tephra deposits from Santorini and compares this dataset to published and new distal data from SE Aegean Sea cores KL49, KL51 and LC21. As a result of 28 proximal-distal tephra correlations, new or revised interpolated eruption age estimates of seven Plinian (Cape Therma 3, Lower Pumice 1 and 2, Cape Thera, Middle Pumice, Vourvoulos, and Upper Scoriae 1) and 17 Inter-Plinian Santorini events of the past ~200 kyrs could be constrained by interpolation of sapropel and oxygen-isotope-tuned chronologies of these cores. Additionally, both proximal-proximal and proximal-distal correlations provide a more robust chronostratigraphic allocation of the Cape Columbos Tuff and Megalo Vouno cinder cone eruptions possibly within the early M9 Inter-Plinian interval (< 121.8 ka) and likely synchronous with the USC1 eruption (80.8 ka), respectively. Results of the tephra studies of marine cores also provide new data on the dispersal of Santorini tephra in a 250 km-transect southeast of Santorini and considerably expands the information available to create isopach maps for the Eastern Mediterranean region.

Distal tephrostratigraphic information of the older interval (i.e., > 200 ka to ~370 ka) of Santorini activity is provided by the evolving terrestrial (crypto)tephra record of the Tenaghi Philippon peat sequence in NE Greece, located ca. 500 km north of Santorini. To date, the Cape Therma 1 tephra and several layers from the M1 and possibly M2 Inter-Plinian interval have been identified and dated by palynostratigraphic constraints (Vakhrameeva et al., 2018, 2019) (Fig. 2).

The improved ~370 ka Santorini proximal and distal tephrostratigraphies are an important step forward in compiling the Eastern Mediterranean tephra framework, but there is still a need for further research. Future research efforts should include:

- EPMA glass fingerprinting of additional minor (Inter-Plinian) Santorini tephra deposits: Such analyses are of particular interest for prominent individual units of the M12, M10, M7, M6, M5, and M2 deposits to detail proximal-proximal and proximal-distal tephra correlations.
- Trace element glass composition of proximal Santorini tephras: Although most Santorini tephras are distinct by their major element glass compositions, there are compositional overlaps which may be resolved by trace element data. Obtaining such data by large-beam (> 10 µm) Laser Ablation (LA) ICP-MS, however, may be difficult due to the large amount of microlites in juvenile clasts (e.g., CTA and MP tephras) or the high vesicularity in silicic tephra shards (e.g., LP1 and LP2 tephras). SIMS analysis with spot sizes of 5–10 µm, as already tested on distal Santorini tephra shards in the Tenaghi Philippon record (Vakhrameeva et al., 2018; Wulf et al., 2018), could be a valuable alternative approach.
- Detailing correlations of distal tephras with specific eruption phases: Distal tephra deposits can derive by fallout from either Plinian or PDC (co-ignimbritic) eruption phases, or from both. Glass chemical data of proximal tephra sub-units from some of the major Santorini eruptions (e.g., CR, USC1, LP2, CTM3) have documented chemical variations between Plinian fall and PDC deposits, and this information was used here to correlate distal marine tephras with distinct eruption phases. Therefore, detailed studies on other proximal Santorini deposits would lead to more comprehensive dataset for understanding eruption dynamics.
- Radioisotopic dating of Santorini tephras: ^{40}Ar/^{39}Ar dating of bulk (multi-grain) samples of proximal Santorini tephra may overestimate eruption ages (Druitt et al., 1999). This issue can be overcome by single-grain laser ^{40}Ar/^{39}Ar analyses, where individual xenocrysts can be identified and removed from the dataset via statistical methods (Kraml, 1997). Another option could be combined U-Th disequilibrium/U-Pb and (U-Th)/He zircon dating of Santorini tephras, a method that has been successfully applied to silicic tephras from e.g. central Anatolia and Ciomadul volcano in Romania (e.g., Schmitt et al., 2011; Harangi et al., 2015; Danišík et al., 2017). The newly constrained, interpolated ages of marine Santorini tephras (this study) would be a great way to test and identify systematic errors in any of the radioisotopic methods applied to proximal Santorini tephras to provide independent dates.

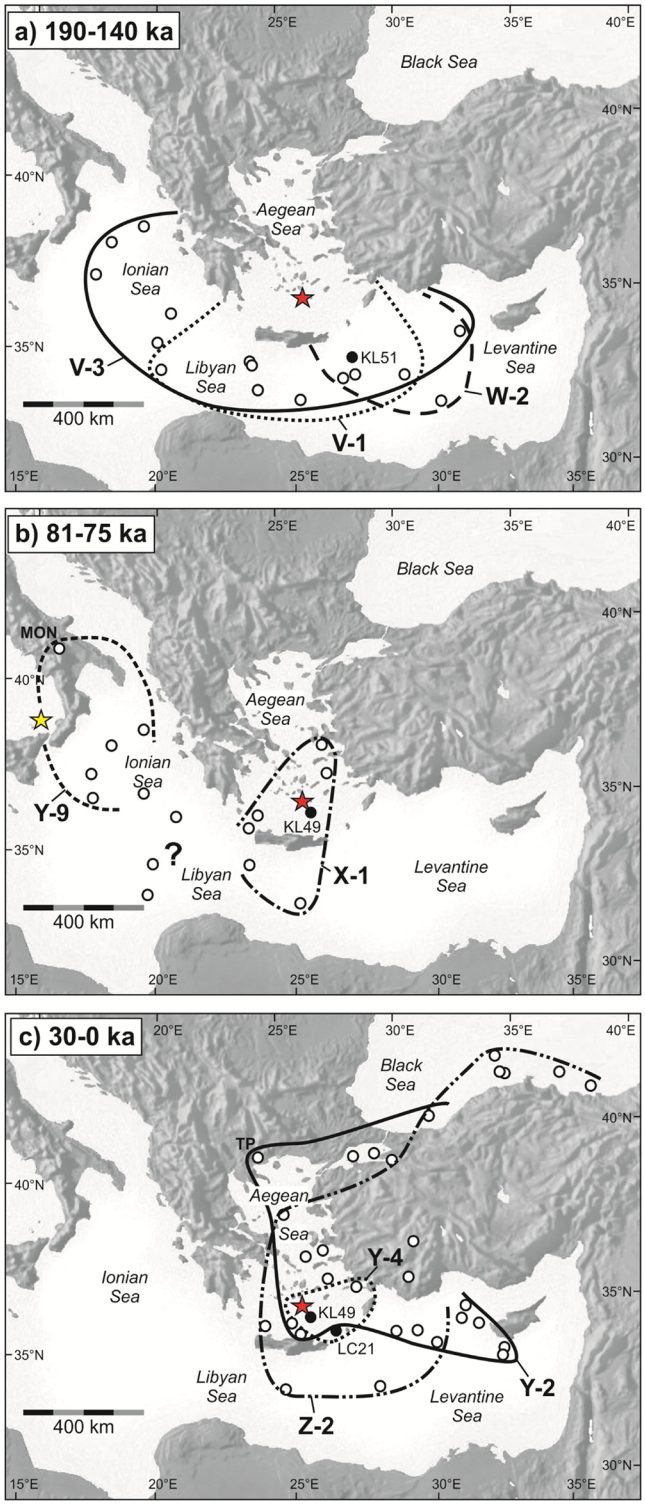

Fig. 10. Dispersal maps of selected, glass geochemically (EPMA) confirmed Santorini tephras. Red star indicates the position of Santorini volcano. **(a)** Distribution of MIS 6 tephras V-3/LP1, V-1/LP2 and W-2/MP; data source: McCoy (1981); Vinci (1985), this study. **(b)** Distribution of MIS 5a tephra X-1/USC1-USC2? and Y-9/Petrazza; data source: McCoy (1981); Vinci (1985); Aksu et al. (2008); Wulf et al. (2004), this study. Yellow star represents the location of Stromboli volcano (Aeolian Islands); the distal-terrestrial sites of Lago Grande di Monticchio (MON) is also shown. **(c)** Distribution of MIS 2 and MIS 1 tephras Y-4/Cape Tripiti?, Y-2/CR and Z-2/MIN; the distal-terrestrial site of Tenaghi Philippon (TP) is also included. Selected data from: Federman and Carey (1980); Vinci (1985); Guichard et al. (1993); Eastwood et al. (1999); Aksu et al. (2008); Kwiecien et al. (2008); Sulpizio et al. (2013); Cullen et al. (2014); Satow et al. (2015); Wulf et al. (2002, 2018) (For interpretation of the references to colour in this figure legend, the reader is referred to the web version of this article.).

- Cryptotephra studies on other marine and terrestrial palaeoenvironmental records: Cryptotephra studies on core LC21 from the southern Aegean Sea (Satow et al., 2015) and in the Tenaghi Philippon peat record from the northern Aegean borderlands (Vakhrameeva et al., 2018, 2019) have demonstrated the great potential to extend the known Santorini tephra dispersal fans. Similar cryptotephra analyses in other long records in the Eastern Mediterranean region (e.g., SE Balkan Peninsula, Asia Minor, Black Sea and Dead Sea) would greatly enhance this knowledge and additionally provide valuable time markers for these records.

Declaration of Competing Interest

None.

Acknowledgements

Special thanks go to Michael Schwarz who did an enormous effort to obtain glass chemical data of tephras from marine cores KL49 and KL51 for a Diploma thesis and who kindly provided his dataset for this study. We thank Sean Whitley (Keele University) for collecting the Cape Tripiti pumice sample used in this study and Monika Doubrava (Heidelberg University) for helping with SAN15 tephra thin-section preparation. We furthermore acknowledge John Spratt (Natural History Museum, London) for his kind assistance in the EPMA analysis of samples SAN16 and SAN17, and Ian Gill (Kingston University) for his skilled mounting and polishing of these samples. Funding for Santorini fieldwork was supported partially by Heidelberg University. JK, MK, AK, JP and PV acknowledge financial support by the Deutsche Forschungsgemeinschaft (DFG; grants KE136/35, KE 136/37, KO4960/3 and PR651/19). Finally, we would like to thank Tim Druitt and Biagio Giaccio for their mindful and constructive comments and suggestions for improving an earlier version of this manuscript.

Appendix A. Supplementary data

Supplementary data associated with this article can be found, in the online version, at http://dx.doi.org/10.1016/j.earscirev.2019.102964.

References

Abu-Zied, R.H., Rohling, E.J., Jorissen, F.J., Fontanier, C., Casford, J.S.L., Cooke, M., 2008. Benthic foraminiferal response to changes in bottom water oxygenation and organic carbon flux in the eastern Mediterranean during LGM to recent times. Mar. Micropaleontol. 67, 46–68.

Aksu, A.E., Jenner, G., Hiscott, R.N., Isler, E.B., 2008. Occurrence, stratigraphy and geochemistry of Late Quaternary tephra layers in the Aegean Sea and the Marmara Sea. Mar. Geol. 252, 174–192.

Albert, P.G., Tomlinson, E.L., Lane, C.S., Wulf, S., Smith, V.C., Coltelli, M., Keller, J., Lo Castro, D., Manning, C.J., Müller, W., Menzies, M.A., 2013. Late glacial explosive activity on Mount Etna: implications for proximal-distal tephra correlations and the synchronisation of Mediterranean archives. J. Volcanol. Geotherm. Res. 265, 9–26.

Albert, P.G., Hardiman, M., Keller, J., Tomlinson, E.L., Smith, V.C., Bourne, A.J., Wulf, S., Zanchetta, G., Sulpizio, R., Müller, U.C., Pross, J., Ottolini, L., Matthews, I.P., Blockley, S.P.E., Menzies, M.A., 2015. Revisiting the Y-3 tephrostratigraphic marker: a new diagnostic glass geochemistry, age estimate, and details on its climatostratigraphical context. Quat. Sci. Rev. 118, 105–121.

Albert, P., Tomlinson, E.L., Smith, V.C., Di Traglia, F., Pistolesi, M., Morris, A., Donato, P., De Rosa, R., Sulpizio, R., Keller, J., Rosi, M., Menzies, M., 2017. Glass geochemistry of pyroclastic deposits from the Aeolian Islands in the last 50 ka: a proximal database for tephrochronology. J. Volcanol. Geotherm. Res. 336, 81–107.

Angelier, J., Lyberis, N., Le Pichon, X., Barrier, E., Huchon, P., 1982. The tectonic development of the Hellenic arc and the Sea of Crete: a synthesis. Tectonophysics 86, 159–196.

Antonopoulos, J., 1992. The great minoan eruption of Thera volcano and the ensuing tsunami in the greek archipelago. Nat. Hazards 5, 153–168.

Bar-Matthews, M., Ayalon, A., Gilmour, M., Matthews, A., Hawkesworth, C.J., 2003. Sea-

land oxygen isotopic relationships from planktonic foraminifera and speleothems in the Eastern Mediterranean region and their implication for paleorainfall during interglacial intervals. Geochim. Cosmochim. Acta 67 (17), 3181–3199.
Bar-Matthews, M., Ayalon, A., Kaufmann, A., 2000. Timing and hydrological conditions of Sapropel events in the Eastern Mediterranean, as evident from speleothems, Soreq cave, Israel. Chem. Geol. 169, 145–156.
Bond, A., Sparks, R.S.J., 1976. The minoan eruption of Santorini, Greece. J. Geol. Soc. Lond. 132, 1–16.
Bronk Ramsey, C., Albert, P.G., Blockley, S.P.E., Hardiman, M., Housley, R.A., Lane, C.S., Lee, S., Matthews, I.P., Smith, V.C., Lowe, J.J., 2015. Improved age estimates for key Late Quaternary European tephra horizons in the RESET lattice. Quat. Sci. Rev. 118, 18–32.
Bruins, H.J., MacGillivray, A., Synolakis, C.E., Benjamini, C., Keller, J., Kisch, H.J., Klügel, A., van der Plicht, J., 2008. Geoarchaeological tsunami deposits at Palaikastro (Crete) and the Late Minoan IA eruption of Santorini. J. Archaeol. Sci. 35 (1), 191–212.
Bruins, H.J., Keller, J., Klügel, A., Kisch, H.J., Katra, I., van den Plicht, J., 2019. Tephra in caves: distal deposits of the Minoan Santorini eruption and the Campanian supereruption. Quat. Int. 499, 135–147.
Çağatay, M.N., Wulf, S., Sancar, Ü., Özmaral, A., Vidal, L., Henry, P., Appelt, O., Gasperini, L., 2015. The tephra record from the Sea of Marmara for the last ca. 70 ka and its palaeoceanographic implications. Mar. Geol. 361, 96–110.
Casford, J.S.L., Rohling, E.J., Abu-Zied, R.H., Jorissen, F.J., Leng, M., Thomson, J., 2003. A dynamic concept for eastern Mediterranean circulation and oxygenation during sapropel formation. Palaeogeogr. Palaeoclimatol. Palaeoecol. 190, 103–119.
Cullen, V.L., Smith, V.C., Arz, H.W., 2014. The detailed tephrostratigraphy of a core from the south-east Black sea spanning the last ~60 ka. J. Quat. Sci. 29 (7), 675–690.
Danišík, M., Schmitt, A.K., Stockli, D.F., Lovera, O.M., Dunkl, I., Evans, N.J., 2017. Application of combined U-Th-disequilibrium/U-Pb and (U-Th)/He zircon dating to tephrochronology. Quat. Geochronol. 40, 23–32.
Davies, S.M., Abbott, P.M., Meara, R.H., Pearce, N.J.G., Austin, W.E.N., Chapman, M.R., Svensson, A., Bigler, M., Rasmussen, T.L., Rasmussen, S.O., Farmer, E.J., 2014. A North Atlantic tephrostratigraphical framework for 130-60 ka b2k: new tephra discoveries, marine-based correlations, and future challenges. Quat. Sci. Rev. 106, 101–121.
De Rijk, A., Hayes, A., Rohling, E.J., 1999. Eastern Mediterranean sapropel S1 interuption and expression of the climatic deterioration around 7 ka BP. Mar. Geol. 153, 337–343.
Devine, J.D., Gardner, J.E., Brack, H.P., Layne, G.D., Rutherford, M.J., 1995. Comparison of microanalytical methods for estimation of H_2O-contents of silicic volcanic glasses. Am. Mineral. 80, 319–328.
Doumas, C., Papazoglou, L., 1980. Santorini tephra from Rhodes. Nature 287, 322–324.
Druitt, T.H., 1985. Vent evolution and lag breccia formation during the Cape Riva eruption of Santorini, Greece. J. Geol. 93, 439–454.
Druitt, T.H., Edwards, L., Mellors, R.M., Pyle, D.M., Sparks, R.S.J., Lanphere, M., Davies, M., Barriero, B., 1999. Santorini Volcano. Geological Society Special Publications, 19. Geological Society, London 165 pp.
Druitt, T.H., Mellors, R.A., Pyle, D.M., Sparks, R.S.J., 1989. Explosive volcanism on Santorini, Greece. Geol. Mag. 126 (2), 95–126.
Druitt, T.H., Sparks, R.S.J., 1982. A proximal ignimbrite breccia facies on Santorini, Greece. J. Volcanol. Geotherm. Res. 13, 147–171.
Druitt, T.H., Francalanci, L., Fabbro, G., 2015. Field Guide to Santorini Volcano. MeMoVolc Short Course. Santorini: pp. 56. .
Eastwood, W.J., Pearce, N.J.G., Westgate, J.A., Perkins, W.T., Lamb, H.F., Roberts, N., 1999. Geochemistry of Santorini tephra in lake sediments from Southwest Turkey. Glob. Planet. Change 21, 17–29.
Edwards, L., 1994. Magma Cyclicity and Isotopic Variation on Santorini Volcano, Aegean Sea, Greece. PhD Thesis. University of Bristol 372 pp.
Fabbro, G.N., Druitt, T.H., Scaillet, S., 2013. Evolution of the crustal magma plumbing system during the build-up to the 22-ka caldera-forming eruption of Santorini (Greece). Bull. Volcanol. 75, 767.
Federman, A.N., Carey, S.N., 1980. Electron microprobe correlation of tephra layers from Eastern Mediterranean abyssal sediments and the island of Santorini. Quat. Res. 13, 160–171.
Fletcher, W.J., Müller, U., Koutsodendris, A., Christanis, K., Pross, J., 2013. A centennial-scale record of vegetation and climate variability from 312 to 240 ka (Marine Isotope Stages 9c-a, 8 and 7e) from Tenaghi Philippon, NE Greece. Quat. Sci. Rev. 78, 108–125.
Fouqué, F., 1879. Santorin et ses éruptions. Masson, Paris.
Friedrich, W.L., 2000. Fire in the Sea. The Santorini Volcano: Natural History and the Legend of Atlantis. Translated by A.R. McBirney. Cambridge University Press, Cambridge.
Friedrich, W.L., Kromer, B., Friedrich, M., Heinemeier, J., Pfeiffer, T., Talamo, S., 2006. Santorini eruption radiocarbon dated to 1627–1600 B.C. Science 312, 548.
Fytikas, M., Kolios, N., Vougioukalakis, G., 1990. Post-Minoan volcanic activity of the Santorini volcano. Volcanic hazard and risk, forecasting possibilities. In: Hardy, D.A. (Ed.), Thera and the Aegean World III. The Thera Foundation, London, pp. 183–198.
Gertisser, R., Preece, K., Keller, J., 2009. The plinian lower pumice 2 eruption, Santorini, Greece: magma evolution and volatile behaviour. J. Volcanol. Geotherm. Res. 186, 387–406.
Giaccio, B., Nomade, S., Wulf, S., Isaia, R., Sottili, G., Cayuoto, G., Galli, P., Messina, P., Sposato, A., Sulpizio, R., Zanchetta, G., 2012. The late MIS 5 Mediterranean tephra markers: a reappraisal from peninsular Italy terrestrial records. Quat. Sci. Rev. 56, 31–45.
Giaccio, B., Niespolo, E.M., Pereira, A., Nomade, S., Renne, P.R., Albert, P.G., Arienzo, I., Regattieri, E., Wagner, B., Zanchetta, G., Gaeta, M., Galli, P., Mannella, G., Peronace, E., Sottili, G., Florindo, F., Leicher, N., Marra, F., Tomlinson, E.L., 2017a. First integrated tephrochronological record for the last ~190 kyr from the Fucino Quaternary lacustrine succession, central Italy. Quat. Sci. Rev. 158, 211–234.
Giaccio, B., Hajdas, I., Isaia, R., Deino, A., Nomade, S., 2017b. High-precision ^{14}C and $^{40}Ar/^{39}Ar$ dating of the Campanian Ignimbrite (Y-5) reconciles the time-scale of climatic cultural processes at 40 ka. Sci. Rep. 7, 45940.
Grant, K.M., Grimm, R., Mikolajewicz, U., Marino, G., Ziegler, M., Rohling, E.J., 2016. The timing of Mediterranean sapropel deposition relative to insolation, sea-level and African monsoon changes. Quat. Sci. Rev. 140, 125–141.
Grant, K.M., Rohling, E.J., Bar-Matthews, M., Ayalon, A., Medina-Elizalde, M., Bronk Ramsey, C., Satow, C., Roberts, A.P., 2012. Rapid coupling between ice volume and polar temperature over the past 150,000 years. Nature 491, 744–747.
Grant, K.M., Rohling, E.J., Westerhold, T., Zabel, M., Heslop, D., Konijnendijk, T., Lourens, L., 2017. A 3 million year index for North African humudity/aridity and the implication of potential pan-African Humid periods. Quat. Sci. Rev. 171, 100–118.
Gudmundsdóttir, E.R., Larsen, G., Björck, S., Ingólfsson, Ó., Striberger, J., 2016. A new high-resolution Holocene tephra stratigraphy in eastern Iceland: improving the Icelandic and North Atlantic tephrochronology. Quat. Sci. Rev. 150, 234–249.
Guichard, F., Carey, S., Arthur, M.A., Sigurdsson, H., Arnold, M., 1993. Tephra from the Minoan eruption of Santorini in sediments of the Black Sea. Nature 363, 610–612.
Harangi, S., Lukács, R., Schmitt, A.K., Dunkl, I., Molnár, K., Kiss, B., Seghedi, I., Novothny, Á., Molnár, M., 2015. Constraints on the timing of Quaternary volcanism and duration of magma residence at Ciomadul volcano, east-central Europe, from combined U-Th/He and U-Th zircon geochronology. J. Volcanol. Geotherm. Res. 301, 66–80.
Hayes, A., Rohling, E.J., De Rijk, A., Kroon, D., Zachariesse, W.J., 1999. Mediterranean planktonic foraminiferal faunas during the Last Glacial cycle. Mar. Geol. 153, 239–252.
Hieke, W., Hemleben, C., Linke, P., Türkay, M., Weikert, H., 1999. Mittelmeer 1998/99, Cruise No. 40, 28 October 1997–10 February 1998. Universität Hamburg.
Hunt, J.B., Hill, P.G., 1996. An inter-laboratory comparison of the electron probe microanalysis of glass geochemistry. Quat. Int. 34-36, 229–241.
Insinga, D.D., Tamburrino, S., Lirer, F., Vezzoli, L., Barra, M., De Lange, G.J., Tiepolo, M., Vallefuoco, M., Mazzola, S., Sprovieri, M., 2014. Tephrochronology of the astronomically-tuned KC01B deep-sea core, Ionian Sea: insights into the explosive activity of the Central Mediterranean area during the last 200 ka. Quat. Sci. Rev. 85, 63–84.
Jochum, K.P., Stoll, B., Herwig, K., Willbold, M., Hofmann, A.W., et al., 2006. MPI-DING reference glasses for in situ microanalysis: new reference values for element concentrations and isotope ratios. Geochem. Geophys. Geosyst. 7 (2), Q02008.
Keller, J., 1981. Quaternary tephrochronology in the Mediterranean region. In: Self, S., Sparks, R.S.J. (Eds.), Tephra Studies. Reidel, Dordrecht, pp. 227–244.
Keller, J., Kraml, M., Schwarz, M., 2000. Dating major volcanic paroxysms within the deep-sea record: the example of the Thera Formation, Santorini, Greece. IAVCEI General Assembly, Bali, Indonesia pp. 16.
Keller, J., Ninkovich, D., 1972. Tephra-Lagen in der Ägäis. Z. Deutsch. Geol. Ges. 123, 579–587.
Keller, J., Ryan, W.B.F., Ninkovich, D., Altherr, R., 1978. Explosive volcanic activity in the Mediterranean over the past 200,000 yr as recorded in deep-sea sediments. Geol. Soc. Am. Bull. 89, 591–604.
Keller, J., Gertisser, R., Reusser, E., Dietrich, V., 2014. Pumice deposits of the Santorini Lower Pumice 2 eruption on Anafi island, Greece: indications for a Plinian event of exceptional magnitude. J. Volcanol. Geotherm. Res. 278-279, 120–128.
Konijnendijk, T.Y.M., Ziegler, M., Lourens, L.J., 2015. On the timing and forcing mechanisms of late Pleistocene glacial terminations: insights from a new high-resolution benthic stable oxygen isotope record of the eastern Mediterranean. Quat. Sci. Rev. 129, 308–320.
Kraml, M., 1997. Laser-$^{40}Ar/^{39}Ar$-Datierungen an distalen marinen Tephren des jungquartären mediterranen Vulkanismus (Ionisches Meer, METEOR-Fahrt 25/4). PhD Thesis. Albert-Ludwigs-Universität Freiburg 216 pp.
Kuehn, S.C., Froese, D.G., Shane, P.A.R., INTAV Intercomparison Participants, 2011. The INTAV intercomparison of electron-beam microanalysis of glass by tephrochronology laboratories: results and recommendations. Quat. Int. 246, 19–47.
Kwiecien, O., Arz, H.W., Lamy, F., Wulf, S., Bahr, A., Röhl, U., Haug, G.H., 2008. Estimated reservoir ages of the Black Sea since the Last Glacial. Radiocarbon 50 (1), 1–20.
Lane, C.S., Brauer, A., Blockley, S.P.E., Dulski, P., 2013. Volcanic ash reveals time-transgressive abrupt climate change during the Younger Dryas. Geology 41, 1251–1254.
Larsen, G., Eiriksson, J., 2008. Late Quaternary terrestrial tephrochronology of Iceland - frequency of explosive eruptions, type and volume of tephra deposits. J. Quat. Sci. 23 (2), 109–120.
Laurenzi, M.A., Villa, I.M., 1987. $^{40}Ar/^{39}Ar$ chronostratigraphy of Vico ignimbrites. Periodico di Mineralogia 56, 285–293.
Lawson, I.T., Swindles, G.T., Plunkett, G., Greenberg, D., 2012. The spatial distribution of Holocene cryptotephras in north-west Europe since 7 ka: implications for understanding ash fall events from Icelandic eruptions. Quat. Sci. Rev. 41, 57–66.
Li, X., Bock, G., Vafidis, A., Kind, R., Harjes, H.P., Hanka, W., Wylegalla, K., van der Meijde, M., Yuan, X., 2003. Receiver function study of the Hellenic subduction zone: imaging crustal thickness variations and the oceanic Moho of the descending African lithosphere. Geophys. J. Int. 155, 733–748.
Lirer, L., Pescatore, T., Booth, B., Walker, G.P.L., 1973. Two Plinian pumice-fall deposits from Somma-Vesuvius, Italy. Geol. Soc. Am. Bull. 84, 759–772.
Lowe, D.J., 2011. Tephrochronology and its application: a review. Quat. Geochronol. 6, 107–153.
Lowe, D.J., Pearce, N.J.G., Jorgensen, M.A., Kuehn, S.C., Tryon, C.A., Hayward, C.L., 2017. Correlating tephras and cryptotephras using glass compositional analyses and

numerical and statistical methods: review and evaluation. Quat. Sci. Rev. 175, 1–44.
Makris, J., 1978. The crust and upper mantle of the Aegean region from deep seismic soundings. Tectonophysics 46, 269–284.
Margari, V., Pyle, D.M., Bryant, C., Gibbard, P.L., 2007. Mediterranean tephra stratigraphy revisited: Results from a long terrestrial sequence on Lesvos Island, Greece. J. Volcanol. Geotherm. Res. 163, 34–54.
Marinatos, S., 1939. The volcanic destruction of minoan crete. Antiquity 13, 425–439.
Marino, G., Rohling, E.J., Rijpstra, W.I., Sangiorgi, F., Schouten, S., Sinninghe Damsté, J.S., 2007. Aegean Sea as driver for hydrological and ecological changes in the eastern Mediterranean. Geology 35, 675–678.
Marino, G., Rohling, E.J., Sangiorgi, F., Hayes, A., Casford, J.S.L., Lotter, A.F., Kucera, M., Brinkhuis, H., 2009. Early and middle Holocene in the Aegean Sea: interplay between high and low latitude climate variability. Quat. Sci. Rev. 28, 3246–3262.
McCoy, F.W., 1981. Areal distribution, redeposition and mixing of tephra within deep-sea sediments of the Eastern Mediterranean sea. In: Self, S., Sparks, R.S.J. (Eds.), Tephra Studies. Nato Advanced Study Institutes Series C 75. Reidel, Dordrecht, pp. 245–254.
Mellors, R.A., Sparks, R.S.J., 1991. Spatter-rich pyroclastic flow deposits on Santorini, Greece. Bull. Volcanol. 53, 327–342.
Mercier, J.L., Sorel, D., Vergely, P., 1989. Extensional tectonic regimes in the Aegean basins during the Cenozoic. Basin Res. 2, 49–71.
Milner, A.M., Roucoux, K.H., Collier, R.E.L., Müller, U.C., Pross, J., Tzedakis, P.C., 2016. Vegetation responses to abrupt climatic changes during the last interglacial complex (marine isotope stage 5) at Tenaghi Philippon, NE Greece. Quat. Sci. Rev. 154, 169–181.
Moller, T., Schulz, H., Hamann, Y., Dellwig, O., Kucera, M., 2012. Sedimentology and geochemistry of an exceptionally preserved last interglacial sapropel S5 in the Levantine Basin (Mediterranean Sea). Mar. Geol. 291-294, 34–48.
Müller, U.C., Pross, J., Tzedakis, P.C., Gamble, C., Kotthoff, U., Schmiedl, G., Wulf, S., Christanis, K., 2011. The role of climate in the spread of modern humans into Europe. Quat. Sci. Rev. 30, 273–279.
Narcisi, B., Vezzoli, L., 1999. Quaternary stratigraphy of distal tephra layers in the Mediterranean - an overview. Glob. Planet. Change 21, 31–50.
Nielsen, C.H., Sigurdsson, H., 1981. Quantitative methods for electron microprobe analysis of sodium in natural and synthetic glasses. Am. Mineral. 66, 547–552.
Ninkovich, D., Heezen, B.C., 1965. Santorini tephra. In: Proceedings of the Seventeenth Symposium of the Colston Research Society. Colston Research Papers 17 Butterworths Scientific Publications, London. pp. 413-452.
Ninkovich, D., Heezen, B.C., 1967. Physical and chemical properties of volcanic glass shards from Pozzuolana Ash, Thera island, and from Upper and Lower Ash Layers in Eastern Mediterranean deep-sea sediments. Nature 213, 582–584.
Pichler, H., Friedrich, W., 1976. Radiocarbon dates of Santorini volcanics. Nature 262, 373–374.
Pross, J., Kotthoff, U., Müller, U., Peyron, O., Dormoy, I., Schmiedl, G., Kalaitzidis, S., Smith, A.M., 2009. Massive perturbation in terrestrial ecosystems of the Eastern Mediterranean region associated with the 8.2 kyr B.P. climatic event. Geology 37, 887–890.
Pross, J., Koutsodendris, A., Christanis, K., Fischer, T., Fletcher, W.J., Hardiman, M., Kalaitzidis, S., Knipping, M., Kotthoff, U., Milner, A.M., Müller, U.C., Schmiedl, G., Siavalas, G., Tzedakis, P.C., Wulf, S., 2015. The 1.35-Ma-long terrestrial climate archive of Tenaghi Philippon, northeastern Greece: Evolution, exploration and perspectives for future research. Newsl. Stratigr. 48, 253–276.
Rach, O., Brauer, A., Wilkes, H., Sachse, D., 2014. Delayed hydrological response to Greenland cooling at the onset of the Younger Dryas in western Europe. Nat. Geosci. 7, 109–112.
Reck, H., 1936. Santorini: Der Werdegang eines Inselvulkans und sein Ausbruch 1925-1928. Verlag von Dietrich Reimer, Berlin.
Regattieri, E., Giaccio, B., Nomade, S., Francke, A., Vogel, H., Drysdale, R.N., Perchiazzi, N., Wagner, B., Gemelli, M., Mazzini, I., Boschi, C., Galli, P., Peronace, E., 2017. A Last Interglacial record of environmental changes from the Sulmona Basin (central Italy). Palaeogeogr. Palaeoclimatol. Palaeoecol. 472, 51–66.
Roeser, P.A., Franz, S.O., Litt, t., Ülgen, U.B., Hilgers, A., Wulf, S., Wennrich, V., Ön, S.A., Viehberg, F., Cagatay, N., Melles, M., 2012. Lithostratigraphic and geochronological framework for the paleoenvironmental reconstruction of the last ~36 ka cal BP from a sediment record from Lake Iznik (NW Turkey). Quat. Int. 274, 73–87.
Rohling, E.J., Cane, T.R., Cooke, M., Sprovieri, M., Bouloubassi, I., Emeis, K.C., Schiebel, R., Kroon, D., Jorissen, F.J., Lorre, A., Kemp, A.E.S., 2002. African monsoon variability during the previous interglacial maximum. Earth Planet. Sci. Lett. 202, 61–75.
Rohling, E.J., Sprovieri, M., Cane, T.R., Casford, J.S.L., Cooke, M., Bouloubassi, I., Emeis, K.C., Schiebel, R., Hayes, A., Jorissen, F.J., Kroon, D., 2004. Reconstructing past planktic foraminiferal habitats using stable isotope data: a case history for Mediterranean sapropel S5. Mar. Micropaleontol. 50, 89–123.
Rotolo, S.G., Scaillet, S., La Felice, S., Vita-Scaillet, G., 2013. A revision of the structure and stratigraphy of pre-Green Tuff ignimbrites at Pantelleria (Strait of Sicily). J. Volcanol. Geotherm. Res. 250, 61–74.
Santacroce, R., Cioni, R., Marianelli, P., Sbrana, A., Sulpizio, R., Zanchetta, G., Donahue, D.J., Joron, J.L., 2008. Age and whole rock-glass compositions of proximal pyroclastics from the major explosive eruptions of Somma-Vesuvius: a review as a tool for distal tephrostratigraphy. J. Volcanol. Geotherm. Res. 177, 1–18.
Satow, C., Tomlinson, E.L., Grant, K.M., Albert, P.G., Smith, V.C., Manning, C.J., Ottolini, L., Wulf, S., Rohling, E.J., Lowe, J.J., Blockley, S.P.E., Menzies, M.A., 2015. A new contribution to the Late Quaternary tephrostratigraphy of the Mediterranean: Aegean Sea core LC21. Quat. Sci. Rev. 117, 96–112.
Scaillet, S., Vita-Scaillet, G., Rotolo, S.G., 2013. Millennial-scale phase relationships between ice-core and Mediterranean marine records: insights from high-precision $^{40}Ar/^{39}Ar$ dating of the Green Tuff of Pantelleria, Sicily Strait. Quat. Sci. Rev. 78, 141–154.
Schmitt, A.K., Danišík, M., Evans, N.J., Siebel, W., Kiemele, E., Aydin, F., Harvey, J.C., 2011. Acigöl rhyolitic field, Central Anatolia (part 1): high-resolution dating of eruption episodes and zircon growth rate. Contrib. Mineral. Petrol. 162, 1215–1231.
Schwarz, M., 2000. Tephrakorrelation im östlichen Mittelmeer (Meteor M40/4 Kerne). Diploma thesis. Albert-Ludwigs-Universität Freiburg 257 pp.
Schwarz, M., Kraml, M., Keller, J., 1999. Tephrochronology of meteor M40/4 cores in the Eastern Mediterranean. EUG 10 Strasbourg (France) 1999, Terra Nova 10 abstract supplement 1. J. Conf. Abstr. 4, 178–179.
Simmons, J.M., Cas, R.A.F., Druitt, T.H., Folkes, C.B., 2016. Complex variations during a caldera-forming Plinian eruption, including precursor deposits, thick pumice fallout, co-ignimbrite breccias and climactic lag breccias: The 184 ka Lower Pumice 1 eruption sequence, Santorini, Greece. J. Volcanol. Geotherm. Res. 324, 200–219.
Smith, P.E., York, D., Chen, Y., Evensen, N.M., Walter, R.C., 1996. ^{40}Ar-^{39}Ar dating of Late Pleistocene volcanic glass from Santorini: a Theran Hyalo-Sphenochron. Eos Trans. Am. Geophys. Union 77 (46).
Sparks, R.S.J., Wilson, C.J.N., 1990. The Minoan deposits: a review of their characteristics and interpretation. In: Hardy, D.A. (Ed.), Thera and the Aegean World III. The Thera Foundation, London, pp. 89–99.
St. Seymour, K.S., Christanis, K., Bouzinos, A., Papazisimou, S., Papatheodorou, G., Moran, E., Dénès, G., 2004. Tephrostratigraphy and tephrochronology in the Philippi peat basin, Macedonia, Northern Hellas (Greece). Quat. Int. 121, 53–65.
Sullivan, D.G., 1988. The discovery of Santorini Minoan tephra in western Turkey. Nature 333, 552–554.
Sulpizio, R., Alcicek, M.C., Zanchetta, G., Solari, L., 2013. Recognition of the Minoan tephra in the Acigöl Basin, western Turkey: implications for inter-archive correlations and fine ash dispersal. J. Quat. Sci. 28 (4), 329–335.
Tartaris, A.A., 1964. The Eocene in the semi-metamorphosed basement of Thera Island. Bull. Geol. Soc. Greece 6, 232–238.
Thorarinsson, S., 1944. Tefrokronologiska studier pa Island. Geografiska Analer 1–215.
Tomlinson, E.L., Smith, V.C., Albert, P.G., Aydar, E., Civetta, L., Cioni, R., Cubukcu, E., Gertisser, R., Isaia, R., Menzies, M.A., Orsi, G., Rosi, M., Zanchetta, G., 2015. The major and trace element glass compositions of the productive Mediterranean volcanic sources: tools for correlating distal tephra layers in and around Europe. Quat. Sci. Rev. 118, 48–66.
Vakhrameeva, P., Koutsodendris, A., Wulf, S., Fletcher, W.J., Appelt, O., Knipping, M., Gertisser, R., Trieloff, M., Pross, J., 2018. The cryptotephra record of the Marine Isotope Stage 12 to 10 interval (460-335 ka) at Tenaghi Philippon, Greece: Exploring chronological markers for the Middle Pleistocene of the Mediterranean region. Quat. Sci. Rev. 200, 313–333.
Vakhrameeva, P., Wulf, S., Koutsodendris, A., Tjallingii, R., Fletcher, W.J., Appelt, O., Ludwig, T., Knipping, M., Trieloff, M., Pross, J., 2019. Eastern Mediterranean volcanism during Marine Isotope Stages 9 to 7e (335–235 ka): Insights based on cryptotephra layers at Tenaghi Philippon, Greece. J. Volcanol. Geotherm. Res. 380, 31–47.
Vespa, M., Keller, J., Gertisser, R., 2006. Interplinian explosive activity of Santorini volcano (Greece) during the past 150,000 years. J. Volcanol. Geotherm. Res. 153, 262–286.
Vinci, A., 1985. Distribution and chemical composition of tephra layers from Eastern Mediterranean abyssal sediments. Mar. Geol. 64, 143–155.
Vitaliano, C.J., Vitaliano, D.B., 1974. Volcanic Tephra on Crete. Am. J. Archaeol. 78 (1), 19–24.
Wastegård, S., Gudmundsdóttir, E., Lind, E.M., Timms, R.G.O., Björck, S., Hannon, G.E., Olsen, J., Rundgren, M., 2018. Towards a holocene tephrochronology for the Faroe Islands, North Atlantic. Quat. Sci. Rev. 195, 195–214.
Watkins, N.D., Sparks, R.S.J., Sigurdsson, H., Huang, T.C., Federman, A., Carey, S., Ninkovich, D., 1978. Volume and extent of the Minoan tephra from Santorini volcano: new evidence from deep-sea cores. Nature 271, 122–126.
Watts, W.A., Allen, J.R.M., Huntley, B., 1996. Vegetation history and palaeoclimate of the last glacial period at Lago Grande di Monticchio, southern Italy. Quat. Sci. Rev. 15, 133–153.
Wulf, S., Kraml, M., Kuhn, T., Schwarz, M., Inthorn, M., Keller, J., Kuscu, I., Halbach, P., 2002. Marine tephra from the Cape Riva eruption (22 ka) of Santorini in the Sea of Marmara. Mar. Geol. 183, 131–141.
Wulf, S., Brauer, A., Kraml, M., Keller, J., Negendank, J.F.W., 2004. Tephrochronology of the 100 ka lacustrine sediment record of Lago Grande di Monticchio (southern Italy). Quat. Int. 122, 7–30.
Wulf, S., Keller, J., Paterne, M., Mingram, J., Lauterbach, S., Opitz, S., Sottili, G., Giaccio, B., Albert, P.G., Satow, C., Tomlinson, E.L., Viccaro, M., Brauer, A., 2012. The 100-133 ka record of Italian explosive volcanism and revised tephrochronology of Lago Grande di Monticchio. Quat. Sci. Rev. 58, 104–123.
Wulf, S., Ott, F., Slowinski, M., Noryskiewicz, A.M., Dräger, N., Martin-Puertas, C., Czymzik, M., Neugebauer, I., Dulski, P., Bourne, A.J., Blaszkiewicz, M., Brauer, A., 2013. Tracing the Laacher See Tephra in the varved sediment record of the Trzechowskie palaeolake in central Northern Poland. Quat. Sci. Rev. 76, 129–139.
Wulf, S., Hardiman, M.J., Staff, R.A., Koutsodendris, A., Appelt, O., Blockley, S.P.E., Lowe, J.J., Manning, C.J., Ottolini, L., Schmitt, A.K., Smith, V.C., Tomlinson, E.L., Vakhrameeva, P., Knipping, M., Kotthoff, U., Milner, A.M., Müller, U.C., Christanis, K., Kalaitzidis, S., Tzedakis, P.C., Schmiedl, G., Pross, J., 2018. The marine isotope stage 1-5 cryptotephra record of Tenaghi Philippon, Greece: Towards a detailed tephrostratigraphic framework for the Eastern Mediterranean region. Quat. Sci. Rev. 186, 236–262.
Zanchetta, G., Sulpizio, R., Roberts, N., Cioni, R., Eastwood, W.J., Siani, G., Caron, B., Paterne, M., Santacroce, R., 2011. Tephrostratigraphy, chronology and climatic events of the Mediterranean basin during the Holocene: an overview. Holocene 21 (1), 33–52.